JOURNAL OF GEOPHYSICAL RESEARCH, VOL. 112, D23301, doi:10.1029/2005JD006214, 2007

Click Here for Full Article

Isotopic analysis of aerosol sulfate and nitrate during ITCT-2k2: Determination of different formation pathways as a function of particle size

N. Patris,[1,2] S. S. Cliff,[3] P. K. Quinn,[4] M. Kasem,[1] and M. H. Thiemens[1]

Received 11 May 2005; revised 5 June 2007; accepted 12 July 2007; published 1 December 2007.

[1] The triple isotopic composition of oxygen in sulfate and nitrate, and the sulfur isotopic composition of the sulfate fine fraction, have been measured on size-segregated aerosol samples collected at Trinidad Head, coastal California, alongside the ITCT-2k2 campaign in April–May 2002. The isotopic anomaly $\Delta^{17}O = \delta^{17}O - 0.52 \times \delta^{18}O$ has been determined in both sulfate and nitrate and was used as a specific tracer of the formation pathways of these species. Coarse mode sulfate in all samples exhibited a small but significant $\Delta^{17}O$ anomaly indicating either uptake or in situ formation of secondary sulfate on sea spray. Non-sea-salt sulfate $\Delta^{17}O$ in the coarse fraction is consistent with (1) either primarily coagulation of finer sulfate particles, when $\Delta^{17}O$ is low in all size fractions, or (2) ozone-driven oxidation of SO_2 within the sea spray, as observed in the relatively higher $\Delta^{17}O$ in coarse particles compared to fine. It is proposed that triple-isotope measurements of sulfate oxygen can be used to quantify the budget of in situ sea spray nss-SO_4 formation. The $\Delta^{17}O$ measured in size-resolved nitrate revealed, for the first time, differences in the nitrate formation budget as a function of particle size in a given air mass. The coarse particle nitrate possessed a higher $\Delta^{17}O$, suggesting a relatively larger N_2O_5 hydrolysis contribution to the nitrate formation budget compared to fine particles where homogeneous formation is more important. We conclude that the complete isotope ratio analysis may provide a basis for future modeling of the formation and transformation processes of the soluble aerosol, based on direct observation of the mechanisms.

Citation: Patris, N., S. S. Cliff, P. K. Quinn, M. Kasem, and M. H. Thiemens (2007), Isotopic analysis of aerosol sulfate and nitrate during ITCT-2k2: Determination of different formation pathways as a function of particle size, *J. Geophys. Res.*, *112*, D23301, doi:10.1029/2005JD006214.

1. Introduction

[2] Several measurement campaigns have recently combined a wealth of techniques (analytical chemistry, satellite observations, meteorology, modeling) to explicitly examine the couplings between chemistry, atmospheric transport, radiative budget, and air quality (e.g., ACE-Asia, PEM-Tropics, INDOEX, ITCT, ICARTT, GoMACCS). These international efforts have confirmed that large interactions exist between atmospheric chemistry and the radiative budget of the atmosphere. These programs have been instrumental in illustrating the importance of transport at regional to intercontinental scales and the associated phenomena. They have also demonstrated that these processes are extraordinarily complex and highly specific to a given region (e.g., *Ramanathan et al.* [2001], *Huebert et al.* [2003], *Fehsenfeld et al.* [2006], and joint papers).

[3] Large domains of the atmospheric physicochemistry are still inadequately described in models because of the absence of relevant data, obtainment of which is hence highly desirable. The interactions between atmospheric chemistry and aerosol microphysics is one such domain, especially the processes controlling the formation of the ubiquitous sulfate and nitrate aerosols. Recent modeling efforts focused on these interactions [e.g., *van den Berg et al.*, 2000; *Tie et al.*, 2003; *Alexander et al.*, 2005]. The implications of this chemistry on the global climate and air quality are important and models would benefit a fine description of the processes [*Gong and Barrie*, 2003; *Boucher and Pham*, 2002; *Pham et al.*, 2005]. The purpose of the present work is to use isotopic data to contribute relevant observations regarding sources, formation and transformation mechanisms affecting the aerosol burden in the atmosphere.

[4] In recent years, the Stable Isotope Laboratory of the University of California San Diego (UCSD) has developed

[1]Department of Chemistry and Biochemistry, University of California, San Diego, La Jolla, California, USA.
[2]Now at Institut de Recherche pour le Développement, UR Great Ice, Montpellier, France.
[3]Department of Applied Sciences, University of California, Davis, California, USA.
[4]Pacific Marine Environmental Laboratory, NOAA, Seattle, Washington, USA.

Copyright 2007 by the American Geophysical Union.
0148-0227/07/2005JD006214$09.00

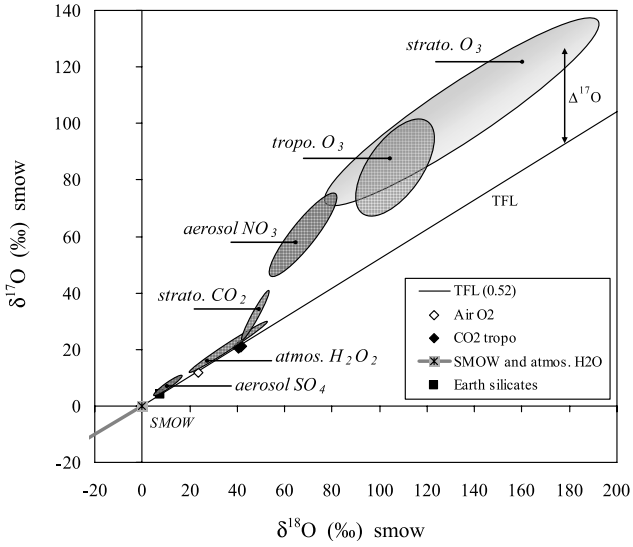

Figure 1. Schematic domains for 3-isotope plots of a number of oxygenated species from Earth's surface and atmosphere. The box legend shows materials falling on the Terrestrial mass-dependent Fractionation Line (TFL). Figured as ovals and labeled in italics are a number of atmospheric compounds showing a mass-independent anomaly $\Delta^{17}O$, defined as the distance from the TFL along the $\delta^{17}O$ axis on the 3-isotope plot. The figure is based on MIF measurements from *Lee and Thiemens* [2001], *Michalski et al.* [2003], *Krankowsky et al.* [1995], *Johnston and Thiemens* [1997], *Schueler et al.* [1990], *Savarino and Thiemens* [1999], *Thiemens et al.* [1995], *Lämmerzahl et al.* [2002], and *Krankowsky et al.* [2007].

a highly original and specific isotope tool capable of resolving complex processes in atmospheric chemistry, especially aerosol formation, transformation, and transport [*Lee and Thiemens*, 2001; *Michalski et al.*, 2003; *Alexander et al.*, 2005]. Specifically, the isotopic Mass-Independent Fractionations (MIF), whereby isotope distributions deviate from statistical laws of mass-dependent relations between isotopomers, are utilized in atmospheric studies. The MIF arise during highly specific physicochemical processes in the atmosphere in isotope systems with three or more stable isotopes, i.e., multiratio (as opposed to "single-ratio isotope systems" where only 2 stable isotopes are measured) isotope systems. The effect is known to occur in oxygen and sulfur isotopic systems and has been observed in a wide variety of atmosphere-cycled compounds (Figure 1). Several reviews of the causes, effects, and potential applications of the MIF in the atmosphere have been recently published [*Thiemens*, 1999; *Thiemens et al.*, 2001; *Thiemens*, 2002; *Johnson et al.*, 2002; *Brenninkmeijer et al.*, 2003].

[5] In oxygen, the ^{17}O anomaly, denoted $\Delta^{17}O$, is defined as the deviation from the conventional mass-dependent-fractionation law relating ^{17}O and ^{18}O abundances in oxygenated compounds:

$$\Delta^{17}O = \delta^{17}O - k \times \delta^{18}O, \quad (1)$$

where the factor $k \approx 0.52$ (actually ranging from 0.50 to 0.529, depending on the molecular mass of the oxygen-bearing molecule and on the process causing the fractionation) defines the slope of the Terrestrial Fractionation Line ($\delta^{17}O \approx 0.52 \times \delta^{18}O$), along which lie most terrestrial oxygenated compounds (e.g., surface and atmospheric water, air O_2, igneous and sedimentary rocks (Figure 1)) within the limited spread caused by processes characterized by slightly differing k factors. The variations in the expression and in the coefficient of the Terrestrial Fractionation Line depend upon the governing fractionation processes and the speciation of the oxygen. Recent papers [e.g., *Young et al.*, 2002; *Miller*, 2002; *Kaiser et al.*, 2004; *Luz and Barkan*, 2005] discuss the intricacies of these expressions in detail.

[6] Ozone formation is a major source of $\Delta^{17}O$ in the atmosphere. The MIF arises partly from molecular symmetry properties, and partly from zero point energy differences in the triatomic transition complex (O_3^*) that enhance the stabilization of the asymmetric ($^{17,18}O^{16}O^{16}O$) isotopomers over the symmetric one ($^{16}O^{16}O^{16}O$) during ozone formation, regardless of the substituted isotope ^{17}O or ^{18}O [*Gao and Marcus*, 2001]. The overall effect is a near equal enrichment in ^{17}O and ^{18}O isotopes, rather than the canonical ~0.52 relation. Gas phase formation of H_2O_2 is another, though lesser source of $\Delta^{17}O$ in the atmosphere [*Savarino and Thiemens*, 1999]. These unique isotopic signatures provide a highly sensitive and unique probe of chemical transformation processes and reaction mechanisms, as the isotopic anomaly is transferred between oxygenated compounds, e.g., from reactant to product in a chemical reaction. Subsequent classical isotope fractionations do not alter the $\Delta^{17}O$ value, or at least only marginally depending on the actual value of k (equation (1)) and the extent of the mass-dependent fractionation. Dilution by the addition of the same species with different isotopic composition, or by isotope exchange with different species, are the only "classical" mass-dependent mechanisms capable of markedly modifying the amount of ^{17}O anomaly in a given compound.

[7] Similarly, in the sulfur system, ^{33}S and ^{36}S anomalies are defined as the deviation from the mass-dependent fractionations compared to $\delta^{34}S$. Nonzero $\Delta^{33}S$ and $\Delta^{36}S$ anomalies have been observed in sedimentary rocks older than 2.09 billion years [*Farquhar et al.*, 2000a]. The origin of these anomalies is thought to be linked to short-wavelength (UV) photochemistry of SO_2, and as such provides a potential tracer of upper tropospheric or stratospheric contributions to the sulfate burden of the present-day troposphere [*Romero and Thiemens*, 2003; *Baroni et al.*, 2007].

[8] Recent isotopic studies have revealed significant mass-independent oxygen isotopic compositions in aerosol sulfates and nitrates [*Lee and Thiemens*, 2001; *Michalski et al.*, 2003], as well as anomalous sulfur compositions in ^{33}S and ^{36}S relative to the ^{34}S in aerosol SO_4 [*Romero and Thiemens*, 2003]. The oxygen isotopic anomalies of particulate sulfate and nitrate are transferred to the product during the oxidation reaction of their precursors (SO_2 and NO_x) by anomalous oxidants, e.g., O_3 and/or H_2O_2 [*Savarino et al.*, 2000; *Michalski et al.*, 2003]. Oxidation processes, and especially ozone chemistry, are heavily involved in soluble aerosol formation and aging processes. The study of the mass-independent signatures of oxygen in atmospheric

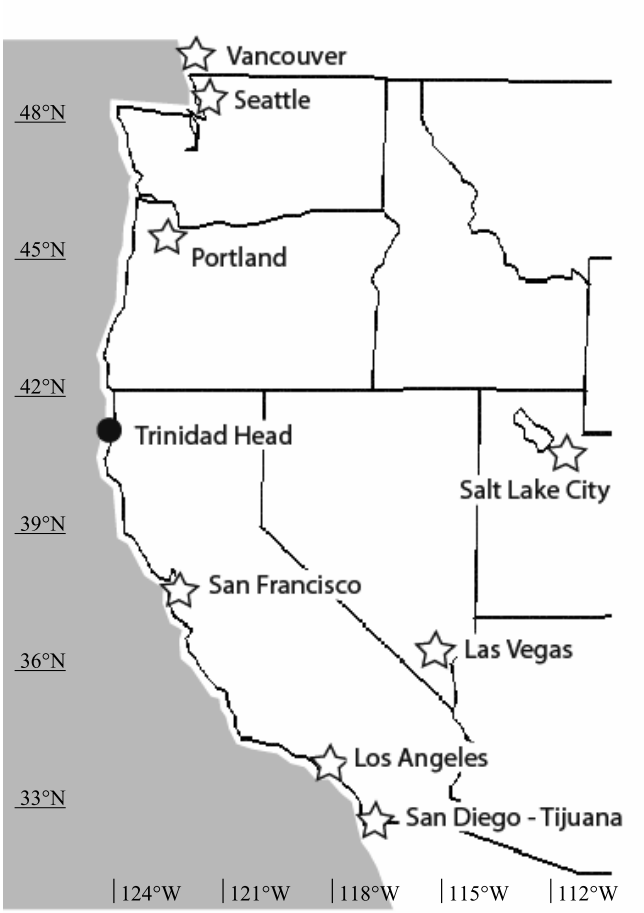

Figure 2. Map of the West Coast of North America showing the location of the Trinidad Head sampling site (solid circle) and the major urban areas within 1200 km (open stars).

sulfate and nitrate has lead to new understandings of their atmospheric chemistry that could not have been obtained by single isotope ratio ($\delta^{18}O$) measurement [*Thiemens et al.*, 2001]. In particular, the ^{17}O anomaly has been used to quantify the different oxidative pathways leading to the formation of sulfate and nitrate, and especially the part of the aqueous phase versus gas phase chemistry [*Savarino et al.*, 2000; *Michalski et al.*, 2003; *Alexander et al.*, 2005].

[9] The present work reports observations of sulfate and nitrate isotopic compositions on a sequential series of size-segregated aerosols collected during the ITCT-2k2 campaign at Trinidad Head, in coastal northern California. The multiratio isotope observations are discussed as a way to providing new details on the mechanisms governing aerosol formation and ageing processes.

2. Sampling and Methods

2.1. ITCT-2k2 Context, Site Description, and Sampling Strategy

[10] Events of trans-Pacific transport of dust and pollution, originating in Asia, are known to occur occasionally during springtime [*Husar et al.*, 2001; *VanCuren and Cahill*, 2002; *DeBell et al.*, 2004]. Recently, transport of a persistent plume was evidenced throughout the year [*VanCuren*, 2003]. The Intercontinental Transport and Chemical Transformation (ITCT-2k2) experiment was a major multiagency campaign focusing on the long-range transport of pollutants from Asia to North America. In particular, the campaign focused on the transformation processes occurring during transport and the subsequent impact on global climate and regional air quality in North America. The ITCT-2k2 operations took place in April and May of 2002, and combined a spectrum of ground-based and airborne observations, satellite data, model forecasting and data integration (http://esrl.noaa.gov/csd/ITCT/2k2/) [*Parrish et al.*, 2004]. The primary ground-based site of study was located at Trinidad Head (41.05°N, 124.15°W, 107 m.a.s.l.), a coastal site of northern California which is clear of direct local urban influence (Figure 2). At this site, we collected aerosol for isotopic analysis during the ITCT-2k2 activities.

[11] Observational and modeling data demonstrated that the ground site at Trinidad Head received very little direct influence from Asian emissions during the period of the campaign, particularly for short-lived gaseous species and aerosols [*Allan et al.*, 2004; *Millet et al.*, 2004; *VanCuren et al.*, 2005]. The most notable influences were essentially "background" contributions to long-lived gases [*Goldstein et al.*, 2004]. Therefore the description of the physicochemical state of the aerosol load observed at Trinidad Head corresponds predominantly to "normal conditions" under which anthropogenic influence is likely to have a regional significance.

[12] One Andersen-Instrument high-volume flow total particulate sampler was used for aerosol collection, operated at a nominal rate of 40 cfm, or 68 m^3 hr^{-1}, and equipped with a 4-stage impactor allowing aerodynamic size segregation of the particles at ambient relative humidity. Glass-fiber filters (4 slotted and one total "backup" filter) were used to collect particles, with cutoff equivalent aerodynamic diameters of 7.2, 3.0, 1.5, and 0.9 μm. The sampler was installed on a 10 m scaffold tower. The sampler operated continuously during 48 to 72-hour periods for each sample collection, thus averaging diurnal patterns. A total of 11 size-segregated aerosol samples were collected, between 24 April and 21 May 2003. Only the last sample was collected over a 25-hour period, which resulted in smaller quantities compared to the rest of the series. Table 1 presents a detailed description of the samples.

2.2. Chemical and Isotopic Analysis

[13] The filters were extracted in 40 mL ultrapure (Millipore) water and sonicated for 1 hour. The extracts were then filtered, and aliquoted for Ion Chromatography (I.C.) determination of anions (Cl^-, Br^-, NO_3^-, SO_4^{2-}, oxalate) and cations (Na^+, K^+, NH_4^+, Mg^{2+}, Ca^{2+}). The major anions (Cl^-, NO_3^-, SO_4^{2-}) were quantified at UCSD with a precision of ±10%. The I.C. quantification of cation and minor anion concentration was performed at the Pacific Marine Environmental Laboratory (PMEL-NOAA) with a precision of ±5%. The SO_4^{2-} and NO_3^- ions were then isolated by I.C., on a high-capacity setup which allows loading and elution

Table 1. Sample Descriptions

Sample	Date	Sampling Duration, hours	6-Day Back Trajectory[a]	$[SO_4]$,[c] $\mu g/m^3$	$[NO_3]$,[c] $\mu g/m^3$
TH 1	24–26 Apr	48	N-E Asia, Manchuria, Bering Sea, Alaska	1.59	1.23
TH 2	26–28 Apr	53	Alaska, N-E Pacific	0.88	0.54
TH 3	28–30 Apr	48	N-E Pacific, coastal BC, coastal USA[b]	0.82	0.73
TH 4	30 Apr to 2 May	48	Alaska, coastal BC, coastal USA[b]	1.16	0.92
TH 5	2–5 May	71	Aleutian, N-E Pacific	1.17	0.42
TH 6	5–8 May	68	N-E Pacific, Canadian north, coastal USA[b]	0.83	0.37
TH 7	8–11 May	75	Vancouver/Seattle area, coastal BC and USA[b]	1.17	0.50
TH 8	11–14 May	55	N-E Pacific, coastal BC, coastal USA[b]	1.40	0.95
TH 9	14–17 May	88	Aleutian, N-E Pacific	1.29	0.43
TH 10	17–20 May	75	N-E Pacific	0.81	0.45
TH 11	20–21 May	25[d]	N-E Pacific	0.76	0.55

[a]Six-day back trajectories calculated by HYSPLIT model (http://www.arl.noaa.gov/ready/hysplit4.html); results displayed for indicative purpose only, by large regional domains.
[b]"Coastal USA" refers to coastal Washington, Oregon, and northern California; back trajectories from Trinidad Head always arrive from the northwest quarter.
[c]Bulk concentrations for sulfate and nitrate, sum of all impactor stages and backup filters (±10%).
[d]TH-11 has been collected for half as long as other samples.

of large volumes of solution. The acidic SO_4^{2-} and NO_3^- solutions obtained were subsequently neutralized to silver salt solutions of Ag_2SO_4 and $AgNO_3$ using a Dionex *AMMS III* cation exchange membrane. The silver salts were then freeze-dried in quartz boats.

[14] The silver sulfate samples were pyrolyzed at ~1020°C to form Ag°, SO_2 and O_2, and Isotope Ratio Mass Spectrometry (IRMS) was performed on the GC-purified O_2. The SO_2 product from this pyrolysis (obtained with a typical yield of ~95%) was converted to H_2SO_4 in a concentrated H_2O_2 solution for subsequent sulfur isotope analysis. The sulfate obtained was precipitated as $BaSO_4$, and converted to Ag_2S and then SF_6, following a method thoroughly described in the literature [e.g., *Farquhar et al.*, 2000b; *Romero and Thiemens*, 2003]. IRMS of sulfur was performed on the GC-purified SF_6.

[15] Likewise, the silver nitrate samples were pyrolyzed at ~520°C to form Ag°, NO_x and O_2, which was then purified and analyzed by IRMS. Both mass-dependent and anomalous isotopic standards were used for calibration, and corrections were applied to the measured O_2 isotopic data to account for the NO_x-O_2 isotopic fractionation [*Michalski et al.*, 2002].

[16] Oxygen obtained from the pyrolysis of the samples was measured by mass spectrometry on a Finnigan MAT-251 against a reference gas O_2 calibrated in both ^{18}O and ^{17}O with respect to the international standard V-SMOW. The ratios $^{34}O_2/^{32}O_2$ and $^{33}O_2/^{32}O_2$ were used to calculate $\delta^{18}O$ and $\Delta^{17}O$ in both sulfate and nitrate. Replicate analyses of laboratory and international standards yielded a standard deviation of ±0.5‰ and ±0.1‰ for $\delta^{18}O$ and $\Delta^{17}O$ respectively. Nonanomalous materials (e.g., analytical grade Fisher sodium sulfate) were tested for the $\Delta^{17}O$ measurement accuracy, and gave consistent zero $\Delta^{17}O$ anomalies ($\Delta^{17}O = -0.01 \pm 0.06$‰, n = 10). Technical and analytical details on O-isotope analyses of sulfate and nitrate are given by *Savarino et al.* [2001] and *Michalski et al.* [2003], respectively, with slight procedural differences. Sulfur isotopes were measured in the product SF_6 on a Finnigan-MAT 252. The ratios $^{34}S/^{32}S$ and $^{33}S/^{32}S$ were used to calculate $\delta^{34}S$ and $\Delta^{33}S$ ($\Delta^{33}S = \delta^{33}S - 0.5155 \times \delta^{34}S$), with respective standard deviations of ±0.05‰ and ±0.03‰ [*Farquhar et al.*, 2000b].

3. Results and Discussion

3.1. Soluble Aerosol Chemistry

3.1.1. Sulfate and Nitrate Concentrations and Size Distributions

[17] The bulk aerosol concentrations of sulfate and nitrate are given in Table 1. The ranges observed of 0.76–1.59 $\mu g\ m^{-3}$ for $[SO_4]$ and 0.37–1.23 $\mu g\ m^{-3}$ for $[NO_3]$ are typical of the coastal boundary layer in the northern hemisphere under no influence of direct anthropogenic emissions [e.g., *Savoie et al.*, 2002; *Malm et al.*, 2004]. (The labels "SO_4" and "NO_3" subsequently refer to the sulfate and nitrate in the aerosol or atmospheric context, regardless of their ionic or neutral, salty or acidic, state.) These levels and their variability are comparable with observations from other groups using different analytical techniques (PILS and AMS) and differing time resolutions for sample collection at the site [*Allan et al.*, 2004; *Tang et al.*, 2004]. The PILS and AMS measurements detected submicron nitrate levels about 0.1 to 0.2 $\mu g\ m^{-3}$, and submicron sulfate about 0.5 to 1.5 $\mu g\ m^{-3}$ on 48 hour averages, which is reasonably close to our findings (Figures 3a and 3b). Our reporting of higher nitrate and sulfate levels compared to colocated experimental reports is explained by the fact that the other techniques deployed focused on micron and submicron fractions and used a cyclone to cut off coarse particles [*Tang et al.*, 2004].

[18] The size distributions of aerosol sulfate and nitrate are displayed in Figures 3a and 3b. The very clear bimodal distribution observed in sulfate was dominated by mass by the submicron mode (backup filter, or stage 5, <0.9 μm diameter), with the less abundant coarse mode corresponding typically to sea spray (stages 1–2). The submicron fraction of sulfate constituted on average 35% (±10%) of the total sulfate mass, and as much as 50% on 2 occurrences (corresponding to samples TH4 on 30 April to 2 May and TH8 on 11–14 May). These samples contained two of the highest total $[SO_4]$ levels observed during the campaign (bulk sulfate concentrations of 1.16 and 1.40 $\mu g\ m^{-3}$ for TH4 and TH8, respectively). Generally speaking, it

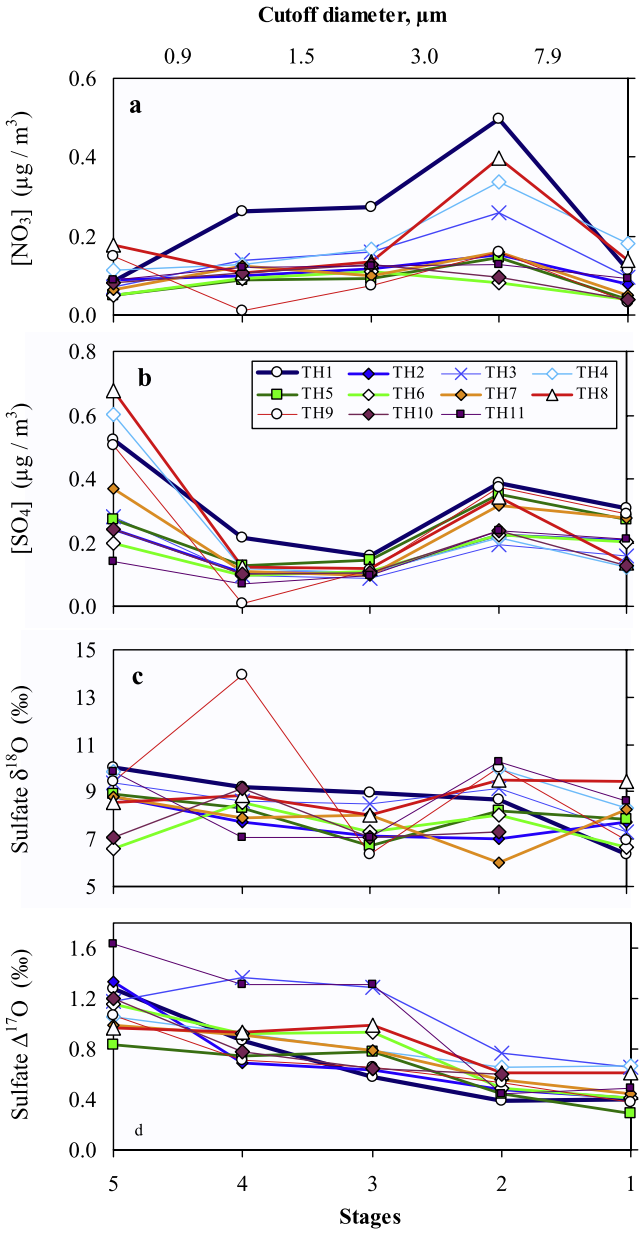

Figure 3. Size distribution (at ambient relative humidity) of the sulfate and nitrate aerosols during the ITCT-2k2 sampling campaign, and oxygen isotopic compositions of sulfate. (a) Nitrate concentrations. (b) Sulfate concentrations. (c) Sulfate $\delta^{18}O$. (d) Sulfate $\Delta^{17}O$. Cutoff equivalent aerodynamic diameters are 7.2, 3.0, 1.5, and 0.9 μm for stages 1 to 4, respectively.

can be seen in Figure 3b that the variability of the fine mode $[SO_4]$ is larger than that of the coarse mode, which indicates that variation in the bulk sulfate aerosol load was predominantly controlled by the fine mode. Nitrate on the other hand was found to be essentially unimodal, centered about stage 2 ($\sim$3–7 μm aerodynamic diameter).

[19] The origin of these size distributions is reasonably well known. Sulfate follows a clear bimodal distribution largely reflecting the two main processes controlling aerosol sulfate formation in the coastal boundary layer: primary sulfate through sea-spray generation, and secondary sulfate derived from SO_2 oxidation and gas-to-particle conversion. Sulfur dioxide itself can have either a direct (as a primary pollutant) or indirect (as the product of atmospheric oxidation of reduced S-species) anthropogenic origin, or result from natural emissions, mainly volcanic exhalations or biogenic DMS oxidation. Secondary sulfate can be produced either by homogeneous oxidation initiated by OH:

$$\text{(R1a)} \qquad SO_2 + OH(+M) \rightarrow HSO_3(+M)$$

$$\text{(R1b)} \qquad HSO_3 + O_2 \rightarrow SO_3 + HO_2$$

$$\text{(R1c)} \qquad SO_3 + H_2O(+M) \rightarrow H_2SO_4(g)(+M),$$

or through aqueous phase reactions of the aerosol:

$$\text{(R2a)} \qquad SO_2(g) + H_2O(liq) \rightarrow SO_2(aq)$$

$$\text{(R2b)} \qquad SO_2(aq) + \text{oxidant} \rightarrow SO_4^{2-}$$

(with SO_2 (aq) = H_2SO_3 + HSO_3^- + SO_3^{2-}), where "oxidant" is mainly either dissolved O_3 or H_2O_2. Other oxidants that play a lesser role in aqueous phase oxidation of SO_2 in the atmosphere include O_2 (oxidation catalyzed by metal) or HO_2NO_2. Because of its low vapor pressure, H_2SO_4 (g) has the capacity to form new particles, or condenses on the existing aerosol.

[20] Nitrate is essentially a secondary species in the atmosphere, the major end product of the nitrogen oxides oxidative chemistry. This is particularly true for atmospheres free of major crustal influence that could otherwise provide mineral nitrates to the primary aerosol load. In the marine boundary layer, the only potential primary source that has been detected is that of alkyl-nitrates in tropical and subtropical regions [*Chuck et al.*, 2002]. The back trajectories showed that the air masses reaching Trinidad Head in April–May 2002 were free of such influences. Secondary nitrate can form in the gas phase following homogeneous reactions via the sequence:

$$\text{(R3)} \qquad NO_2 + OH(+M) \rightarrow HNO_3(g)(+M)$$

$$\text{(R4a)} \qquad NO_2 + O_3 \rightarrow NO_3^{\bullet} + O_2$$

$$\text{(R4b)} \qquad NO_3^{\bullet} + \text{VOC, DMS} \rightarrow HNO_3(g).$$

[21] Gaseous HNO_3 rapidly condenses onto aerosol surfaces. Nitrate can also form through heterogeneous hydrolysis:

$$\text{(R5a)} \qquad NO_2 + NO_3^{\bullet} \leftrightarrow N_2O_5$$

$$\text{(R5b)} \qquad N_2O_5 + H_2O(liq) \rightarrow 2\,HNO_3(aq).$$

[22] In both the homogeneous and heterogeneous cases, formation of nitrate involves, or is followed by deposition on the surface of an existing aerosol. As a consequence, particulate nitrate is found in particle modes dominating the surface distribution, which typically resides in the micron range. The deposition of gaseous nitric acid is also favored onto more alkaline aerosol, which can shift its distribution toward coarse particles in the marine atmosphere [*Sievering et al.*, 2004; *Alexander et al.*, 2005].

[23] Halogen oxides may also play a significant role in both sulfate and nitrate formation [*Sander et al.*, 1999; *von Glasow et al.*, 2002], but because of the many gaps in our knowledge on the implications of this chemistry at the isotope level, in this work we will only consider the classical HO_x-NO_x-SO_x-O_x scheme described through reactions ((R1a)–(R5b)) in our oxidation budgets. Consideration of the possible repercussions of the halogen chemistry on the oxygen isotope tracers remain highly speculative at the moment, but lines of thought may be drawn from our current knowledge, and are presented in Appendix A.

3.1.2. Air Mass Origins

[24] As previously mentioned, the extensive observation of an Asian dust plume was one of the main motivations for the ITCT-2k2 experiment. Continuous particulate sampling and subsequent elemental measurements were carried out by the University of California–Davis with an 8-stage Rotating DRUM Impactor sampler (RDI) at the site during the campaign, with a typical time resolution of 3 hours [*Perry et al.*, 2004; *VanCuren et al.*, 2005]. Elemental measurements were utilized to characterize the potential transport of dust and crustal material, and allowed for the identification of source regions [*VanCuren et al.*, 2005]. Soil concentration was calculated from the assumed stoichiometric oxides of soil containing elements using the algorithm: [SOIL] = 2.20[Al] + 2.49[Si] + 1.63[Ca] + 2.42[Fe] + 1.94[Ti] [*Malm et al.*, 1994]. Long-range soil transport derived from Asia occurred early in the campaign, between the onset of the RDI measurements on 21 and 26 April [*VanCuren et al.*, 2005]. During that early period, bulk [SOIL] (sum of the 8 impactor stages) ranged between 1575 and 5776 ng m^{-3} (arithmetic mean ~2300 ng m^{-3}). From 26 April on, bulk [SOIL] was always between 300 and 2000 ng m^{-3} (arithmetic mean ~850 ng m^{-3}).

[25] Considering the isotope sampling, only the first sample (TH1), collected 24–26 April, was under measurable influence from an Asian-derived dust-laden air mass, which is inadequate to directly assess the influence of Asian emissions upon the isotopic character of the sulfate and nitrate aerosols. However, it is notable that this soil-influenced air mass had the highest levels of both sulfate and nitrate (Table 1), consistent with entrainment of anthropogenic pollution from large urban centers in Asia at the onset of the long-range transport. The size distributions of sulfate and nitrate were affected to some extent by the large aerosol density in the aged air mass. Nitrate concentration levels in intermediate stages 4, 3, and 2 (0.9 to 7.2 μm aerodynamic diameter) were substantially higher during the 24–26 April period (0.26, 0.27, and 0.50 μg m^{-3}, respectively) than during the rest of the campaign (almost double compared to the TH2 to TH10 stage averages shown in Figure 3a). Sulfate in the micron to supermicron range (stages 1 to 4) was higher on TH1 than during the remainder of the campaign, albeit only slightly. The enhancement is more pronounced on the micron aerosol bin (stage 4), where the sulfate level ($[SO_4]$ = 0.22 μg m^{-3}) more than doubled the mean value for this size fraction observed during the rest of the campaign (0.10 ± 0.03 μg m^{-3} for TH2 to TH10). However, the finest fraction of aerosol sulfate and nitrate in the dust-impacted sample was within the same concentration range as the nonimpacted ones.

[26] The HYSPLIT back trajectories (http://www.arl.noaa.gov/ready/hysplit4.html) calculated from Trinidad Head for several altitude levels (from surface up to 500 m above ground at Trinidad Head) show rapid trans-Pacific transport during the 22–26 April period, the origin of the air masses 6–7 days prior to sampling being located unambiguously in the northeast Asia region (Gobi, N.E. China, Siberia). Asian-derived soil evidenced at the site from 20 to 26 April is explained by downward mixing of free tropospheric air associated with strong frontal activity [*VanCuren et al.*, 2005]. For the remainder of the study, 6-day back trajectories never reach west of the 180° meridian. The 6-day trajectories reveal air mass origins either from the Bering Sea–Aleutian area (TH2, TH5), the northeast Pacific (TH3, TH4, TH8, TH9, TH10), and one sample from the Canadian north (TH6). The trajectories then generally followed the coast lines of Canada and northwest USA, with two exceptions during which the air followed a clear easterly flow upon arrival above Trinidad Head (TH10 and TH11). Air trajectories for sample TH7 clearly passed over urban areas (Seattle-Vancouver). There is no obvious trend in the bulk chemistry or in the size distribution of sulfate and nitrate with the geographical origin of the air masses. Indeed the dominant aerosol at the Trinidad Head site during ITCT-2k2 was essentially a mixture of sea salt and aged combustion [*VanCuren et al.*, 2005]. The sum of [Na] and [Cl] averaged 2000 ng m^{-3}, nearly twice the soil average of 1200 ng m^{-3}, for the entire sampling period. In addition to the geographical origin of air masses over the span of a few days, the wind speed near the collection site was important as it controlled the amount of mixing with local pollutants in the air mass. *Tang et al.* [2004] identified periods when the surface wind speeds were low and CO and NO_x levels increased, presumably because of local sources. Those periods of enhanced local contribution encompassed the samples TH3 and TH8.

[27] With these fundamentals in mind, high-precision multi isotope ratio measurements are utilized to describe more precisely the processes affecting aerosol formation and ageing during transport to the Trinidad Head sampling site.

3.2. Oxygen and Sulfur Isotopes of Aerosol Sulfate

[28] The complete isotopic analysis of sulfate provides information on the SO_4 formation pathway (O isotopes), as well as the source and oxidation processes of sulfur during atmospheric transport (S isotopes). All impactor stages from each sample were analyzed individually for O isotopes, constituting a complete set of over fifty $\delta^{18}O$ and $\Delta^{17}O$ size-resolved measurements. Sulfur isotopes have been measured on several fine fractions (backup filters) as a preliminary test of the utility of multiratio isotope analysis of sulfur.

Table 2. Sulfate O-Isotope Analyses From Size-Segregated Aerosols Collected at Trinidad Head During ITCT-2k2 (n = 52)[a]

	Stage 5 (Fine)	Stage 4	Stage 3	Stage 2	Stage 1 (Coarse)
$\Delta^{17}O$, ‰, mean	+1.15 ± 0.22	+0.92 ± 0.24	+0.86 ± 0.27	+0.54 ± 0.11	+0.48 ± 0.13
$\delta^{18}O$, ‰, mean	+8.8 ± 1.1	+8.9 ± 1.9	+7.5 ± 0.8	+8.6 ± 1.4	+7.8 ± 0.9

[a]Mean isotope values calculated for each impactor stage on 10 samples, and a total of 52 isotope analyses. Cutoff equivalent aerodynamic diameters: 0.9 μm (stage 4), 1.5 μm (stage 3), 3.0 μm (stage 2), and 7.2 μm (stage 1).

3.2.1. Sulfate $\delta^{18}O$

[29] The size distribution of sulfate $\delta^{18}O$ exhibits little sensitivity to aerosol size when the entire data set is considered (Figure 3c and Table 2). The stage-averaged $\delta^{18}O$ values ranged between +7.5‰ and +8.9‰ with respect to Standard Mean Ocean Water (SMOW), which is close to, but slightly lighter than the sea-salt-sulfate value of +9.6‰ [*Longinelli and Craig*, 1967]. These values are typical of reported $\delta^{18}O$ values for aerosol sulfate, although on the light end of the observed range. Recent studies of sulfate aerosol in the Pacific North American region reported $\delta^{18}O$ values in the range +6‰ to +15‰ in the Vancouver area [*Norman et al.*, 2004], from +8.4‰ to +15.2‰ and +5.3‰ to +13.1‰, respectively, for fine and coarse coastal aerosols in La Jolla (San Diego area) [*Lee and Thiemens*, 2001], and an extensive study of continental total sulfate deposition in southwest USA averaged at $\delta^{18}O$ = +11.2 ± 1.9‰ [*Bao and Reheis*, 2003]. The factors controlling sulfate $\delta^{18}O$ include the oxidation pathway and the isotopic composition of the reactants, especially water (both as H_2O and OH, and also controlling the $\delta^{18}O$ in SO_2 with which isotopic equilibrium is fast [*Holt et al.*, 1981]). The lighter $\delta^{18}O$ in the Trinidad Head aerosol sulfate compared to previous studies in southern California may be due to secondary sulfate that was formed at mid-to-high latitudes where atmospheric water is generally depleted in heavy isotopes. Within a sample, differences between aerosol size fractions can vary by as much as 3‰, but no systematic trend with size is observed (Figure 3c). The size-dependent contributions of sea-salt sulfate do not control $\delta^{18}O$ variations, because the isotopic ranges of sea-salt and non-sea-salt sulfate overlap.

3.2.2. Total Sulfate $\Delta^{17}O$ Distributions

[30] In contrast to the single isotope ratio, $\Delta^{17}O$ is highly sensitive to particle size, with a nonzero positive value in the coarse fraction ($\Delta^{17}O$ ranging from +0.2 to +0.75‰, mean $\Delta^{17}O$ = +0.48‰), and a larger positive value in fine particles (ranging from +0.8 to +1.6‰, mean $\Delta^{17}O$ = +1.15‰). The amount of $\Delta^{17}O$ varies quasi-linearly with size within each sample (Figure 3d). The resolution of the size separation of the aerosol under ambient humidity during 48 hour collection periods is not ideal. It appears that the changing meteorological conditions affecting the amount of liquid water (relative humidity, temperature), and therefore the diameter of the particles, produced a widening of sulfate particle distribution on the impactor stages. The resultant overlapping of size fractions may eventually have contributed to the quasi-linear isotope variations observed with respect to the impaction stages.

[31] The temporal variations of sulfate $\Delta^{17}O$ isotope anomalies are plotted along with $\delta^{18}O$ and sulfate concentrations for all size fractions in Figure 4. Both the concentration (top) and the $\Delta^{17}O$ (middle) time series are characterized by the same features: coarse mode stages 1 and 2 (particles > 3.0 μm) vary in parallel with each other, and the same is observed for intermediate stages 3 and 4 (0.9 to 3.0 μm). The finer particles (submicron, on stage 5) vary without correlation with the other size fractions. This is significant in that considering the 3 size bins (fine, intermediate and coarse) the isotopic composition of sulfate is apparently sensitive to different processes that govern oxidation pathways, aerosol formation, and transport.

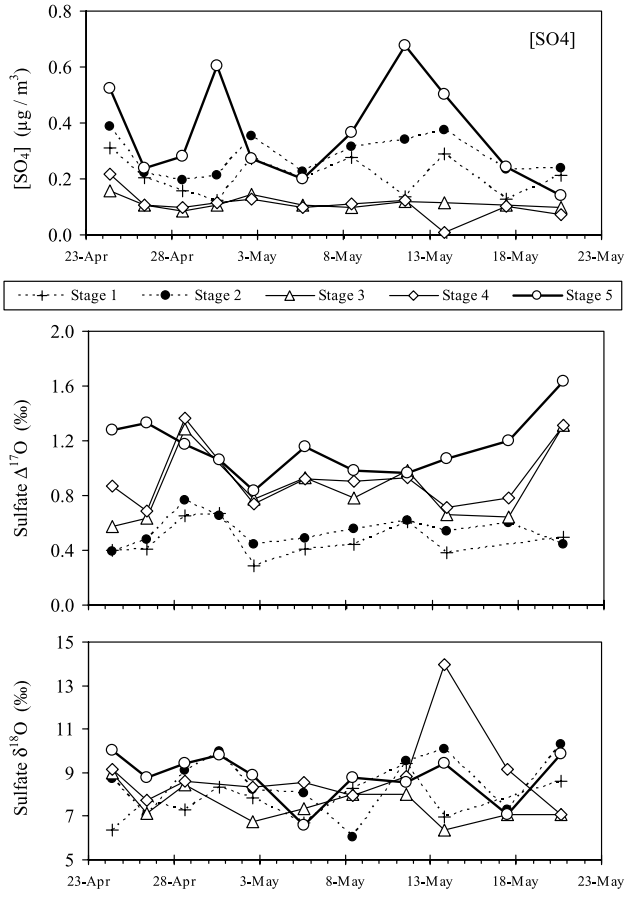

Figure 4. Temporal variations of (top) $[SO_4]$, (middle) sulfate isotope anomaly $\Delta^{17}O$ indicative of aqueous phase formation of the sulfate, and (bottom) $\delta^{18}O$ of sulfate. Submicron particles (stage 5) are indicated by the thick solid line, intermediate fractions (stages 4 and 3) are indicated by the thin solid lines, and supermicron particles (stages 2 and 1) are indicated by the dashed lines. The symbols are placed at the beginning of each sampling period.

Table 3. Non-Sea-Salt Sulfate $\Delta^{17}O$ (‰) From Size-Segregated Aerosols[a]

	Stage 5 (Fine)	Stage 4	Stage 3	Stage 2	Stage 1 (Coarse)
TH 1	+1.5 ± 0.2	+1.5 ± 0.4	+1.6 ± 0.8	*+2.1 ± 2.4*	*+3.9 ± 7.7*
TH 2	+1.7 ± 0.2	+1.5 ± 0.6	+2.1 ± 1.3	*+2.7 ± 3.1*	*+2.8 ± 4.0*
TH 3	+1.4 ± 0.2	+2.2 ± 0.4	+2.7 ± 0.8	+2.6 ± 1.6	*+3.8 ± 4.1*
TH 4	+1.2 ± 0.2	N/A[b]	N/A[b]	+2.4 ± 1.6	+2.3 ± 1.4
TH 5	+1.1 ± 0.2	+1.8 ± 0.8	+3.1 ± 2.2	*+2.4 ± 2.7*	*+2.5 ± 4.7*
TH 6	+1.4 ± 0.2	+2.3 ± 0.9	+2.7 ± 1.3	*+13 ± 70*	*+6.9 ± 24*
TH 7	N/A[c]	+4.3 ± 3.6	+4.1 ± 3.9	*+3.4 ± 4.1*	*+5.6 ± 15*
TH 8	+1.1 ± 0.2	+1.3 ± 0.3	+2.0 ± 0.6	+1.5 ± 0.7	+1.7 ± 0.9
TH 9	+1.4 ± 0.2	N/A[c]	+2.6 ± 1.9	*+3.4 ± 4.2*	*+2.9 ± 4.5*
TH 10	N/A[c]	+1.9 ± 0.8	+2.5 ± 1.8	*+4.2 ± 5.7*	N/A[b]
TH 11	N/A[c]	N/A[c]	N/A[c]	N/A[c]	N/A[c]

[a]Non-sea-salt SO_4 anomaly calculated taking ss-SO_4/Na = 0.25 (mass ratio) and $\Delta^{17}O$ = 0.0‰ for ss-SO_4 [*Bao and Thiemens*, 2000]. Error bars are calculated taking into account uncertainties on isotopic measurements and on sulfate and sodium concentrations. Italics indicate cases in which error bars are equal to or larger than the calculated anomaly.
[b]Isotopic composition not available.
[c]Cation data not available.

[32] To characterize the different populations of aerosol sulfate, one can consider the two extreme size fractions as representative of the two sulfate aerosol modes. In both the supermicron and the submicron size fractions (stages 1 and 5, respectively), the $\Delta^{17}O$ is negatively correlated with the sulfate concentration, more clearly so on the coarse mode (R^2 = 0.70) than on the fine (R^2 = 0.22). In the case of the supermicron particles, the correlation is indicative of a dominating sea-salt component in aerosol sulfate at higher concentrations. As discussed above, the air masses consistently followed a coastal trajectory prior to arrival at Trinidad Head. The oceanic air fetch coupled with local sea spray production near Trinidad Head is responsible for the enhanced levels of low-$\Delta^{17}O$ coarse mode sea-salt-SO_4. However, the significantly larger than zero ^{17}O anomaly of the coarse sulfate indicates that a measurable amount of secondary sulfate is present in this fraction. Secondary sulfate can be integrated into the coarse aerosol either from in situ production of sulfate by aqueous phase chemistry in the sea-spray particles, or from coagulation of finer particles onto sea-spray particles. The finer particulate sulfate would result from cloud or fog processing, i.e., aqueous phase oxidation of SO_2, or from gas-to-particle conversion, i.e., gaseous H_2SO_4 condensation.

3.2.3. Non-Sea-Salt Sulfate $\Delta^{17}O$ Signatures

[33] To determine the nature of secondary sulfate present in the different size fractions, the non-sea-salt component has been evaluated and its isotopic value retrieved from the total sulfate $\Delta^{17}O$ measurements. Sodium was used as the conservative tracer of sea salt, and the sea-salt sulfate proportion was determined using the SO_4/Na mass ratio representative of seawater (ss-SO_4/Na = 0.25). The sea-salt contribution to sulfate was on average ~100%, 95%, 78%, 60%, and 25% in stages 1 to 5 respectively. The relatively high sea-salt content down to the finer fraction may have resulted from the proximity of the sampler to the wave-breaking shore. The isotopic anomaly of non-sea-salt sulfate has been calculated for most individual size bins, except for sample TH11 in which concentration levels were too low to ensure accurate determination of the nss-SO_4 content (Table 3). The uncertainty associated with the non-sea-salt sulfate isotopic determination is higher when the sea-salt contribution to SO_4 is prominent. We calculated the uncertainty for each sample stage by propagating the analytical uncertainties of the SO_4 and Na concentrations assessed by I.C. (±10%), and on the measured $\Delta^{17}O$ of the total sulfate (±0.1‰). The error bars calculated are generally larger for stages 1 and 2 (from ±0.5‰ to several permil units when ss-SO_4 amounts to 80–100% of total sulfate), but are significantly less for the finer size fractions (ranging from ±0.15 to ±0.22‰ for stage 5).

[34] The most striking result of this calculation is the nearly constant value of nss-SO_4 anomaly for the submicron particles: $\Delta^{17}O$ = 1.35 ± 0.20‰ (ranging from 1.07‰ to 1.68‰ on the 8 backup filters for which cation data are available). The intermediate stages or the coarse mode display a much higher variability during the campaign, even though the calculated uncertainties encompass a large range of $\Delta^{17}O$ values. However, two distinct situations can be described: in several samples the non-sea-salt $\Delta^{17}O$ signature is constant within the uncertainties on the 5 size fractions, while in the other cases, there is a clear difference between the nss-SO_4 anomaly in the supermicron particles, and the anomaly in the fine aerosol.

[35] In the cases of samples TH1 and TH2 for instance, a linear correlation is observed between the magnitude of the $\Delta^{17}O$ anomaly and the sea-salt sulfate percentage on the five impaction stages (linear regression coefficients R^2 = 0.986, and 0.977 for TH1 and TH2 respectively, n = 5), suggesting a simple two-component mixing. Figure 5 (left) shows the variation of $\Delta^{17}O$ of total sulfate as a function of the sea-salt sulfate percentage for TH1, TH2, as well as TH10 (only stages 2 to 4 are available). The non-sea-salt sulfate anomaly in those samples is constant (within uncertainties) throughout the size bins (Table 3). In this case, the similar isotopic signatures of fine and coarse particle non-sea-salt sulfate indicate that the particles may have formed following a unique oxidative pathway. This suggests that the excess sulfate present in the coarse fraction may result predominantly from coagulation of fine particles onto the primary particles (dust or sea spray) or from particle growth. Recent modeling studies tend to support these mechanisms as efficient ones provided sufficient time allows for transformation in the air mass before removal [*Raes et al.*, 2000]. Samples TH3, TH6 or TH8, on the other hand, tend to have a higher anomaly on the excess sulfate present in the

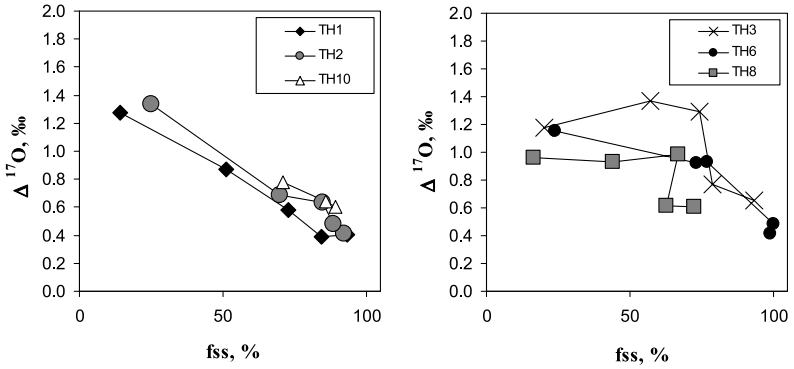

Figure 5. Isotopic anomaly $\Delta^{17}O$ of total sulfate as a function of the sea-salt sulfate percentage (fss). Symbols for each sample are collection stages in consecutive order 5 to 1 (stage 5 corresponds to lower fss, at ~15 to 25%). (left) Samples consistent with a two-component mixing of ss-SO4 and one light-$\Delta^{17}O$ nss-SO_4 (R^2 = 0.986, 0.977, 0.997 for samples TH1, 2 (n = 5), and 10 (n = 3), respectively). (right) Samples inconsistent with a simple two-component mixing, indicating different formation budgets in the supermicron and submicron fractions (R^2 = 0.35, 0.81, and 0.33 for samples TH3, 6, and 8 (n = 5), respectively).

supermicron aerosol, as compared to the fine (Figure 5, right), and do not correspond to a simple 2-member mixing (linear regression coefficients between $\Delta^{17}O$ and the % ss-SO_4 of R^2 = 0.35, 0.81, and 0.33 respectively, n = 5). This observation indicates a different oxidation pathway for the sulfur populating the different aerosol size fractions.

[36] The different formation pathways of atmospheric SO_4 (reactions (R1) and (R2)) incorporate significantly different isotopic compositions in the product sulfate depending on the oxidant involved. The homogeneous gas phase production of H_2SO_4 resulting from SO_2 + OH leads to a strictly mass-dependent sulfate ($\Delta^{17}O$ = 0). The aqueous phase oxidation of SO_2 by either H_2O_2 or O_3, depending on the pH and availability of these reagents, will produce ^{17}O anomalies of varying magnitude. Ozone possesses the largest anomaly in ^{17}O (~25 to 35‰ for tropospheric ozone and generally higher for stratospheric ozone, depending on the location and altitude) [*Schueler et al.*, 1990; *Krankowsky et al.*, 1995, 2007; *Johnston and Thiemens*, 1997; *Lyons*, 2001], while hydrogen peroxide possesses a smaller $\Delta^{17}O$, of the order of +1.5‰ [*Savarino and Thiemens*, 1999]. Aqueous phase oxidation of SO_2 by O_3 favors the partial transfer of this large anomaly to the sulfate, with the transfer of one of the oxygen atoms from the ozone molecule into the SO_4 [*Savarino et al.*, 2000]. In the case of aqueous phase reaction of SO_2 with H_2O_2, *Savarino et al.* [2000] found that the 2 oxygen atoms are transferred from H_2O_2 to the SO_4. However, the anomaly residing in atmospheric H_2O_2 being comparatively much smaller, the ozone oxidation pathway produces sulfate with a notably higher anomaly [*Lee and Thiemens*, 2001]. *Lee and Thiemens* [2001] calculated the amount of $\Delta^{17}O$ in sulfate produced in aqueous phase oxidation at La Jolla (coastal California). They found that the pH of the aqueous phase controls the reaction rates by the two oxidants O_3 (dominant by several orders of magnitude at pH > 6) and H_2O_2 (dominating at pH < 5), and therefore controls the amount of $\Delta^{17}O$ in the SO_4 formed. The expected $\Delta^{17}O$ in the sulfate produced from H_2O_2 or O_3 oxidation ranged between +0.8‰ and +8.6‰ respectively. Taking the non-anomalous aqueous pathway of catalytic oxidation by O_2 into account, *Lee and Thiemens* [2001] calculated that sulfate $\Delta^{17}O$ due to aqueous phase formation ranged from +0.8‰ at pH < 4.5, to +6.8‰ at pH > 6.

[37] In the light of these results, our data suggests that the low $\Delta^{17}O$ of the fine particles non-sea-salt sulfate is indicative of either dominant gas phase production of H_2SO_4 or cloud processing during atmospheric transport. The high non-sea-salt sulfate anomaly indicative of ozone chemistry confirms that this process occurs mostly on the coarse fraction of the aerosol, i.e., sea spray. Moreover, it appears to be a dominant process only intermittently, when favorable conditions are met.

3.2.4. Two Scenarios for Coarse Non-Sea-Salt Sulfate Formation

[38] The present observations lead to a suggestion that depending on the history of the air masses, excess sulfate in the coarse and intermediate fractions may or may not differ isotopically from that of the fine mode. The constant nss-SO_4 anomaly in the coarse fractions of samples TH1 and TH2 is relatively low ($\Delta^{17}O$ = +2.1‰ ± 0.8‰), which indicates either the dominance of the low-pH favored aqueous H_2O_2 oxidation, or a strong contribution of the SO_2 + OH homogeneous reaction. The long-lived fine aerosol in this scenario would constitute most of the coarse particle excess sulfate, specifically by coagulation onto coarse particles. It is interesting to note that the single sample dominated by long-range transport of Asian pollution (TH 1), stands in this category: these sulfate particles had sufficient time to form and interact with dust prior to subsiding to lower altitude. The coagulation process could have occurred during transport. This is consistent with the arguments of *Perry et al.* [2004], which suggested that sulfate associated with particulate soil is responsible for the hygroscopic nature of the observed aerosol at Trinidad Head during ITCT-2k2. We also cannot rule out that the fine particles associated with the dust-laden air mass could have coagulated on sea spray regionally as well, when the aged polluted air mass subsided above the coastal regions of

Table 4. Sulfur Isotopic Compositions of Sulfate for Fine Fractions (Stage 5)[a]

	δ^{34}S, ‰	δ^{34}nssS, ‰	Δ^{33}S, ‰
TH 1	+3.30	+0.37	+0.05
TH 2	+8.55	+4.42	+0.09
TH 4	+7.18	+4.34	+0.04
TH 5	+9.66	+5.81	+0.03
TH 7	+7.88	N/A[b]	+0.06
TH 9	+9.63	+5.89	+0.06
TH 10	+9.37	N/A[b]	+0.10

[a]Sulfur isotopic values δ^{34}S reported on the VCDT scale, for total sulfate (column 1) and for nss-sulfate (column 2). Anomaly Δ^{33}S considered nonsignificant when $\leq$0.10‰.

[b]Cation data not available.

North America, down to atmospheric levels where mixing with sea-spray particles could occur.

[39] The second scenario indicates a proportionally less significant coagulation process to form the coarse fraction non-sea-salt sulfate, and a larger part of in situ SO_2 oxidation in the sea spray. The alkalinity of the fresh sea spray favors a potential SO_2 oxidation with O_3 as a major oxidant [*Sievering et al.*, 1999], which is consistent with the observations that indicate a higher non-sea-salt anomaly in the coarse fraction. Unfortunately, the error bars limit a more accurate determination of this contribution at present. In particular, it is difficult to estimate whether coagulation or condensation of gaseous H_2SO_4 contribute significantly to the coarse non-sea-salt sulfate in this case. However, the results are sufficiently consistent to suggest that ozone oxidation is a major contributor in this size range, while this is not the case in the fine particle population collected at the same time. Ideally, the determination of Δ^{17}O in non-sea-salt sulfate allows for the quantification of the three formation pathways in all size fractions when the uncertainties of chemical and isotopic analyses are minimized. Clearly, future analyses will prove most powerful with the incorporation of high-precision chemical data.

[40] Though essentially qualitative conclusions may be drawn from this study, the present observations provide an operational basis on which a physicochemical modeling of the air mass ageing processes may be carried out. Recent studies have pointed out the potential importance of in situ sulfate formation in the sea spray [*Gurciullo et al.*, 1999; *Laskin et al.*, 2003; *Sievering et al.*, 2004; *Alexander et al.*, 2005]. This process has potential climatic implications, as it may mediate the rate of new particle formation in the marine boundary layer. Indeed, sulfate produced by oxidation of DMS has been hypothesized to be the major natural source of cloud condensation nuclei in remote marine atmospheres, which could in turn regulate the solar radiation available to the marine ecosystems, and play a role in the global cloud cover [*Charlson et al.*, 1987]. The washout of the sulfate precursor SO_2 by sea spray can represent an efficient way to bypass the marine biosphere-climate system feedback loop proposed by *Charlson et al.* [1987] by suppressing part of the DMS oxidation products at the sea surface. *Sievering et al.* [1999, 2004] estimated that O_3 oxidation of SO_2 in alkaline sea spray accounted for as much as 50–75% of the observed coarse excess sulfate (>0.7 μm) at Cape Grim, Tasmania, during the ACE-1 experiment. The measurements of the ^{17}O anomaly of sulfate provides a new way to unambiguously observe this key process, as it is able to differentiate the excess sulfate present in sea spray as either in situ SO_2 oxidation by ozone or fine particle coagulation.

3.2.5. Sulfur Isotopes

[41] Several samples have been analyzed for the sulfur isotope compositions δ^{34}S and Δ^{33}S (Table 4). These are only fine fractions (stage 5), since sea-salt contributions are minor (ranging between 14% and 25% of the total sulfate) and therefore the secondary sulfate may be more clearly resolved. All samples possess no Δ^{33}S anomaly (all < 0.1‰). Following the hypothesis of *Romero and Thiemens* [2003] that sulfur anomalies are due to high-altitude (stratosphere/upper troposphere) contributions from UV sulfur dioxide photolysis, our results indicate that high-altitude source is not a measurable part of the sulfate budget at Trinidad Head during the sampling period.

[42] The single-ratio δ^{34}S is widely used as a tracer of sulfur sources, especially in marine or coastal atmospheres, where sea-salt sulfate (δ^{34}S = 21‰), anthropogenic (0‰ to +7‰), and marine biogenic sources (~18‰) are readily distinguishable [e.g., *Norman et al.*, 1999; *Patris et al.*, 2000, 2002]. Sample TH 1 stands out as having a much lower δ^{34}S (+3.3‰) than the 6 other samples measured (mean δ^{34}S = 8.7 ± 1.0‰). Column 2 of Table 4 reports the δ^{34}S of non-sea-salt sulfate (δ^{34}nssS) for the cases where cation data are available. Again, sample TH1 stands out as having the lowest value (δ^{34}nssS = +0.4‰) out of the 5 samples where cation data are available (mean δ^{34}nssS = 4.2 ± 2.2‰).

[43] In all samples but TH1 non-sea-salt δ^{34}S values are on the high end of the anthropogenic range. These values are consistent with a largely anthropogenic dominant source of sulfur, with or without mixing of DMS-derived sulfate. In this isotopic range the advection of biogenic sulfate cannot be confidently resolved, mostly because of the variability of the anthropogenic end-member. However, the results indicate that the anthropogenic contributor exceeds the marine biogenic one. The observed isotopic values represent the complex and mixed state of the sulfur budget at the site and the variety of contributing sulfur sources. These sources are present in the vicinity of the site, and along the trajectories of the air masses.

[44] Sample TH 1 on the other hand shows a typically anthropogenic signature (δ^{34}nssS = +0.4‰) that can be directly related to the Asian source, consistently with observations of the insoluble part of the aerosol by elemental analysis [*Perry et al.*, 2004]. The isotopic signature close to 0‰ corresponds generally to coal burning, which is a major source of anthropogenic S emissions in China and other regions of Southeast Asia [*Kreutz and Sholkovitz*, 2000; *Pruett et al.*, 2004; *Yu and Park*, 2004]. This result suggests that the conditions of transport prevented any mixing with marine biogenic emissions, particularly the high-altitude level of the transport. This supports the scenario presented earlier, whereby the aged sulfate aerosol interacted with dust during the long-range transport, and possibly also rapidly mixed with fresh sea spray as the air masses subsided over the coastal areas of North America.

[45] The case of sample TH 7 is worth noting as well. Even though the absence of cation data for the finer fraction prevents the nss-SO_4 isotopic determination, and the sea-

Table 5. Nitrate O-Isotope Analyses From Size-Segregated Aerosols Collected at Trinidad Head During ITCT-2k2, Averaged by Impaction Stage

	Stage 1 (Coarse)	Stage 2	Stage 3	Stage 4	Stage 5 (Fine)
$\Delta^{17}O$, ‰, mean	+25.2 ± 2.2	+25.6 ± 1.7	+25.0 ± 1.7	+24.3 ± 2.4	+23.9 ± 2.1
$\delta^{18}O$, ‰, mean	+63.5 ± 5.6	+63.9 ± 4.4	+64.3 ± 4.8	+62.2 ± 6.2	+61.9 ± 5.8

salt content remains high on the intermediate sizes, the calculated $\Delta^{17}O$ for non-sea-salt sulfate is notably higher than the rest of the data set (especially stages 3 and 4, where $\Delta^{17}O$ = +4.1 ± 3.9‰ and +4.3 ± 3.6‰ respectively; see Table 3). The error bars, when I.C. uncertainties are propagated, are too large to draw specific conclusions. However, the results are consistent with the calculated air mass trajectories which traveled above urban centers in the Seattle-Vancouver area, indicating the possible influence of a strongly polluted, ozone-rich environment. *Norman et al.* [2004] recently measured S isotopes of aerosol sulfate in the urban area of Vancouver and found $\delta^{34}S$ = +4.4 to +6.0‰, which is higher than the mean, but within the range of anthropogenic signatures mentioned earlier. As an approximation, the average percentage of sea-salt-sulfate in the fine particles of the other samples (*f*ss = 20%) can be used to estimate the non-sea-salt isotopic signature in this sample. The value thus calculated, δ^{34}nssS = +4.6‰, is not significantly different from the other samples values. These data are in the range reported by *Norman et al.* [2004] for urban aerosol, which further supports our hypothesis that anthropogenic sulfur may be dominant in the fine particles. In this case the high oxygen-17 anomaly adds new information on the chemistry within the air mass.

[46] The clear decoupling of the sulfur isotope data and the oxygen isotope data demonstrates how the two types of isotope tracers provide complementary information on the source terms for sulfur, and on the oxidative history of the sulfate particles for oxygen, all in the same molecule.

3.3. Oxygen Isotopes of Aerosol Nitrate

3.3.1. Nitrate $\Delta^{17}O$ Measurements

[47] Because of the analytical constraints, which require at least 8–10 μmol of nitrate per analysis, the extracts from different stages of each sampling had to be combined to achieve the maximum accuracy in the measurements. Generally stages 1–2 and 4–5 were combined if necessary, or analyzed individually, to provide sufficient amounts for the high-precision multi-isotope ratio measurement, while preserving the size information. The isotopic compositions have been determined for two fractions, namely "fine" (submicron and micron particles) and "coarse" (supermicron) by weight averaging of the corresponding stages for each sampling. The fine fraction includes stages 5 and 4 on all samples, except TH10, which contains stages 5, 4, and 3.

[48] The previous studies of oxygen multi-isotope ratios of atmospheric nitrate exhibited a high enrichment both in $\delta^{18}O$ and in $\Delta^{17}O$, compared to other atmospheric species (Figure 1). The Trinidad Head nitrate samples are likewise enriched. Table 5 shows mean $\delta^{18}O$ and $\Delta^{17}O$ values for nitrate in each stage; keeping in mind that most of the measurements were combinations of contiguous stages, this had a smoothing effect on the variability of the data presented with respect to size. Although the standard deviation of the measurements covers the range of the stage-averaged data, a clear trend is observed with a systematically lower mean $\Delta^{17}O$ anomaly toward the finer aerosol size (Table 5). Table 6 presents the nitrate ^{17}O anomaly for the fine and coarse fractions in each sample. The time series of size-resolved [NO_3], $\delta^{18}O$, and $\Delta^{17}O$ of nitrate are presented in Figure 6. One finds a second trend of $\Delta^{17}O$ decrease with time for both fine and coarse fractions. The linear trend lines of the coarse and fine nitrate $\Delta^{17}O$ indicate both a mean variation of approximately −1.3‰ every 10 days during the course of the campaign, as well as a constant ∼1.5‰ difference between the coarse and fine components.

3.3.2. Nitrate Formation Budgets From $\Delta^{17}O$ Measurements

[49] *Michalski et al.* [2003] defined precise theoretical $\Delta^{17}O$ isotopic signatures for each of the nitrate formation pathways (R3, R4, R5) as a function of the $\Delta^{17}O$ anomaly in the atmospheric ozone involved in the NO_x cycling and oxidation, and by considering the origin of the O atoms in the NO_3 molecule that is produced (i.e., O_3, H_2O,NO_x, HO_x, RO_x). *Michalski et al.* [2003] used a typical tropospheric ozone anomaly of $\Delta^{17}O$ = +35‰, determined by calculation of the fractionation factors associated with chemical reactions and physicochemical parameters relevant to atmospheric conditions [*Lyons*, 2001] and at the high end of the tropospheric ozone isotope measurements

Table 6. Nitrate-$\Delta^{17}O$ Values From Size-Segregated Aerosols Collected at Trinidad Head (n = 31) and Estimated Relative Contributions of Heterogeneous (R3) Nitrate Formation Compared to Homogeneous ((R1) and (R2)) for Fine and Coarse Fractions[a]

		Nitrate $\Delta^{17}O$		% Heterogeneous (R3)	
Sample	Collection Dates	Fine	Coarse	Fine	Coarse
TH 1	24–26 Apr	+25.6‰	+25.7‰	72	74
TH 2	26–28 Apr	+25.3‰	+27.2‰	68	100
TH 3	28–30 Apr	+27.1‰	+27.5‰	98	100
TH 4	30 Apr to 2 May	+23.5‰	+27.0‰	38	97
TH 5	2–5 May	+24.3‰	+26.5‰	51	89
TH 6	5–8 May	+24.9‰	+25.3‰	60	69
TH 7	8–11 May	+23.9‰	+24.5‰	45	54
TH 8	11–14 May	+20.1‰	+24.6‰	0	55
TH 9	14–17 May	+21.8‰	+24.8‰	8	59
TH 10	17–20 May	+25.4‰	+25.7‰	70	74
TH 11	20–21 May	+21.9‰[b]	+21.9‰[b]	9[b]	9[b]

[a]Stages were usually combined to provide sufficient NO_3 amount for $\Delta^{17}O$ measurement. Stage 3 combined with either coarse (stages 1–2) or fine (stages 4–5) modes depending on individual stage amounts. Heterogeneous percent contributions to nitrate formation are in relation to homogeneous (NO_2 + OH and NO3• + HC) nitrate formation; Large uncertainties are expected, due to parameterization (see text).

[b]TH 11, single bulk measurement.

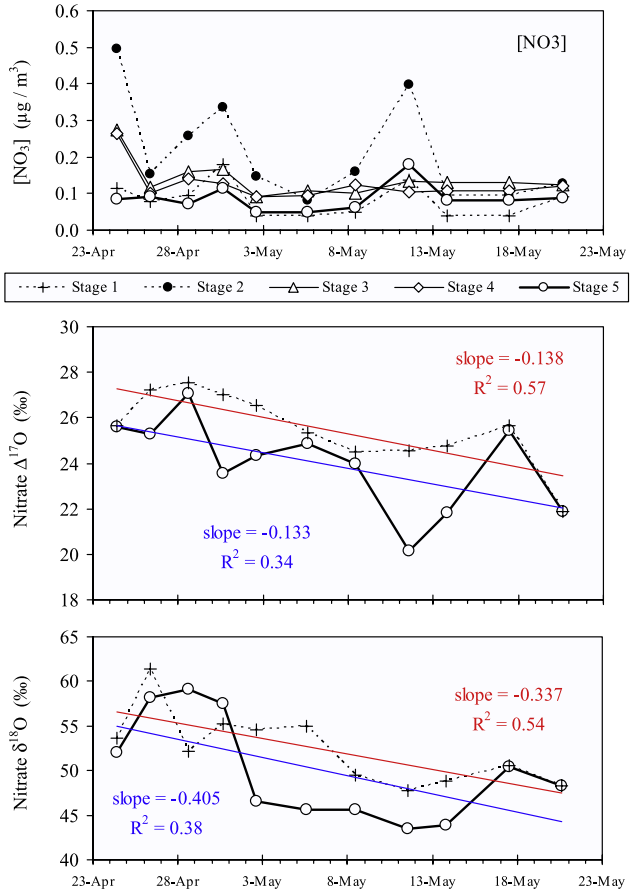

Figure 6. Temporal variations of (top) $[NO_3]$, (middle) nitrate isotope anomaly $\Delta^{17}O$ indicative mainly of the homogeneous (R3) versus heterogeneous (R5a) (R5b) formation of nitrate, and (bottom) nitrate $\delta^{18}O$. In Figure 6 (top), submicron particles (stage 5) are indicated by the thick solid line, intermediate fractions (stages 4 and 3) are indicated by the thin solid lines, and supermicron particles (stages 2 and 1) are indicate by the dashed lines. In Figure 6 (middle and bottom), combined submicron and micron (stages 5, 4, and 3) are indicate by the solid lines, and combined supermicron (stages 3, 2, 1) is indicated by the dashed line. Blue and red lines are linear trend lines for fine and coarse fractions, respectively. The symbols are placed at the beginning of each sampling period. Real sample timing is taken into account in the calculation of the slopes of the trend lines.

[*Krankowsky et al.*, 1995; *Johnston and Thiemens*, 1997]. They have determined that H abstraction by the NO_3• radical (R4) is the pathway yielding the highest nitrate anomaly, ideally equal to that of ozone ($\Delta^{17}O \sim 35‰$), since all precursors other than O_3 (namely the NO_x) are in isotopic equilibrium with O_3, and mass-dependent isotopic fractionations preserve the $\Delta^{17}O$. However, this formation pathway generally plays a lesser role in the nitrate formation budget. *Michalski et al.* [2003] coupled the nitrate $\Delta^{17}O$ measurements with a chemistry model, and estimated the (R4) pathway contribution to be limited, at ~5 (±5)% of the nitrate production year-round at La Jolla, California. The two main nitrate formation pathways (heterogeneous $N_2O_5 + H_2O$ and homogeneous NO_2 + OH) would induce nitrate $\Delta^{17}O$ anomalies of +29.2‰ and +23.3‰, respectively, following *Michalski et al.* [2003]. These isotope signatures are estimated by taking into account O_3 as the exclusive oxidant in NO_2 formation ($NO + O_3 \rightarrow NO_2 + O_2$). The proportion of NO oxidation into NO_2 by ozone and other oxidants (HO_2, RO_2), is a key parameter to consider since it determines the anomaly in the precursor NO_2, which has not yet been directly measured. When HO_2 and RO_2 compete with ozone in the NO_2 formation, the anomaly in NO_2 is diluted in proportion [*Michalski et al.*, 2003]. In the case where 15% of the NO_2 is due to HO_2 or RO_2, the calculated anomalous signatures are $\Delta^{17}O = +25.7‰$ for N_2O_5 hydrolysis (R5), $\Delta^{17}O = +19.8‰$ for the homogeneous NO_2 + OH pathway (R3), and $\Delta^{17}O = +31.5‰$ for the minor NO_3• pathway (R4).

[50] The average difference of 1.5‰ evidenced between fine and coarse particles is rather small, but with respect to the ~6‰ difference between the signature of the homogeneous and heterogeneous pathways, this small difference may represent a significant differential in the formation budgets of fine and coarse nitrate. Likewise, the trend of a decreasing anomaly for both fine and coarse particles as the campaign progressed (trend lines in Figure 6) may be caused by a measurable shift in the NO_3 production pathways. The contribution from nonanomalous crustal nitrate in the isotopic variations can be ruled out, as it would lower the anomaly preferentially in the coarse fraction and especially at sampling periods associated with dust, which is inconsistent with the observations. We can therefore safely consider the aerosol nitrate at Trinidad Head as an exclusively secondary atmospheric compound.

3.3.3. Possible Seasonal Trend in Nitrate Production

[51] As a preliminary approach, we can consider the contribution of the (R4) pathway (NO_3• + DMS, VOC) to be ~5 to 10% of the total nitrate production throughout the sampling period, similar to the estimate by *Michalski et al.* [2003] for the Spring season at La Jolla, another coastal site in California. One can then estimate the relative contributions of the homogeneous (R3) versus heterogeneous (R5) nitrate formation pathways in the fine and coarse size fractions, and their variations with time.

[52] Let us consider first the trend lines for fine and coarse nitrate $\Delta^{17}O$ (respectively blue and red lines in Figure 6) instead of the detailed data. The temporal decrease in the anomaly may correspond to seasonality in the NO_3 formation budget pointed out by *Michalski et al.* [2003] on a year-round study at La Jolla. In winter, limited photochemistry and cooler temperatures are responsible for the dominance of the high-$\Delta^{17}O$ heterogeneous N_2O_5 channel, whereas summer conditions limit the N_2O_5 formation and favor the NO_2 + OH chemical pathway. In addition, the more intense OH chemistry in summer enhances HO_2 and RO_2 levels, which compete with O_3 in the NO oxidation into NO_2. The effect on the isotopes is a dilution of the ozone $\Delta^{17}O$ anomaly in the NO_2 reservoir, hence a lower $\Delta^{17}O$ in the product nitrate. If this peroxy effect is not taken into account, any value lower than +23.3‰ (i.e., cases of TH 8, 9, and 11) would not be explained by an atmospheric origin according to the chemical scheme proposed. In the case described by *Michalski et al.* [2003] at La Jolla, the

RO_2 and HO_2 oxidation of NO ranged from 0% in winter up to ~15% in summer. These values may be used in an empirical way to modulate the NO_2-induced anomaly during the course of the campaign. If α represents the percent of oxidation of NO by ozone as opposed to other species, let us set α = 100% on 21 December and a linear decrease of the parameter so that α = 85% on 21 June. The sampling period thus corresponds to α = 89 ± 1% during the campaign. The homogeneous versus heterogeneous contributions for the two trend lines may then be precisely calculated for the set of parameters chosen. The trend line for the fine fraction indicates an overall minor contribution from the heterogeneous formation (mean 45%, varying from 73% on 24 April to 11% on 21 May), whereas the trend line for the coarse fraction indicates the dominance of this pathway (mean 71%, from ~100% to 40%). It is worth noting that these estimates are only indicative, considering the uncertainties due to the parameters chosen. However, the evidence of temporal variations of the formation pathway budgets is relevant.

[53] The temporal decrease of the heterogeneous pathway and the corresponding increase of the homogeneous nitrate production are attributed here to a seasonal change in chemistry, rather than a change in transport. Indeed back trajectories did not show air masses originating from systematically lower latitudes toward the end of the campaign, as would be needed to explain the stronger OH activity. In fine NO_3 particles the homogeneous and heterogeneous nitrate formations are overall comparable in our estimate (~50% homogeneous OH pathway, compared to ~45% heterogeneous), whereas the coarse fraction is dominated by heterogeneous formation. This result represents the first observation of a differential role of the homogeneous and heterogeneous nitrate formation pathways in different particulate aerosol size fractions in the same air mass. This may have important implications as the size of particles mediates their optical properties and their interactions with solar and earth radiations.

[54] Likewise, the relative contributions for the heterogeneous (R5) versus homogeneous (R3) pathways may be estimated for the individual samples, using the same approximations for the formation of NO_2 by peroxy radical chemistry, and the NO_3• radical pathway (R4 ~ 5–10%). The estimates are reported in the right hand columns of Table 6. The seasonal trend is no longer captured, but the variability at a timescale of 48–72 hours is now considerable, particularly for the fine fraction. The estimated fine nitrate heterogeneous formation fluctuates between being largely dominant and minor, from one sample to the next. The situation with the coarse nitrate is relatively more stable as the heterogeneous pathway is always dominant in samples TH1 to TH10. Large uncertainties are included in these estimates: for instance, a shift in α from 89% to 80%, which would not be considered unrealistic, would result in the reestimation of the heterogeneous pathway by +30 to +40%. Only a complete modeling work integrating all relevant chemical and physical parameters would be able to exploit the observational evidence to produce a quantification of the budget of nitrate formation pathways. The description of the nitrate formation as a function to particle is mainly qualitative at present.

3.3.4. No Clear Link Between Sulfate and Nitrate Chemistries

[55] As in the case of sulfate, one category of samples possesses similar nitrate production budgets in the coarse and fine fractions (e.g., TH 1, 3, 6, 7, 10), while another group of samples reveals large differences between fine and coarse (e.g., TH 2, 4, 5, 8, 9). The two subensembles are not common between nitrate and non-sea-salt sulfate (i.e., when non-sea-salt SO_4 coarse and fine modes are isotopically consistent, nitrate coarse and fine fractions are not always consistent, and vice versa). This is not surprising considering that the processes governing the size distributions of the secondary sulfate and nitrate depend upon their formation mechanisms and are entirely different for the two species. The interactions that exist between the sulfate and nitrate in the presence of sea spray, pointed out by multiple recent studies [e.g., *Alexander et al.*, 2005; *Hwang and Ro*, 2006; *Saul et al.*, 2006], do not imply a simple correlation will exist on the isotopic tracers of formation. In the case of sulfate, either coagulation of fine sulfate particles or in situ oxidation of SO_2 in the aqueous phase is required, whereas uptake of gaseous HNO_3 or N_2O_5 at the surface is the main process that leads to nitrate incorporation into the aerosol. These processes are largely independent from one another even if pH effects may influence the competition between the acid end products.

[56] The differential between coarse and fine fractions observed for the nitrate is relatively less straightforward to explain than in the case of sulfate, where sea spray chemistry plays a major and highly specific role. In the case of nitrate, the N_2O_5 hydrolysis requires water at the surface where N_2O_5 favorably deposits or forms [*Mentel et al.*, 1999; *Karagulian et al.*, 2006; *Anttila et al.*, 2006]. The surface area size distribution in marine and high-latitude environments is typically dominated by particles in the supermicron size range. Frequent cycling of water uptake and loss by the aerosol exposed to various regimes of temperature, pressure, and relative humidity, may distribute the N_2O_5 hydrolysis products over a relatively large size distribution. This smoothing action by the meteorological conditions may affect to a varying degree the ultimate nitrate size distribution. The homogeneous pathways NO_2 + OH (R3) and H-abstraction by the NO_3• radical (R4) also involve condensation of the gaseous HNO_3 onto the surface of a preexisting particle. However, the presence of a water layer at the surface is not required and the acid may also deposit on solid mineral or organic surfaces [*Santschi and Rossi*, 2006; *Vlasenko et al.*, 2006]. The ultimate size distribution of nitrate in the aerosol is therefore governed by parameters that vary with the nature of the precursor of particulate nitrate. These parameters include the gas phase diffusion of the species (N_2O_5, NO_2, NO_3, HNO_3), surface accommodation coefficients that in turn may depend on the physicochemical nature of the aerosol surface, and thermodynamic equilibrium between the aerosol and gas phases. Different size distributions are therefore to be expected in the products resulting from the different formation pathways. This isotopic study is the first one to present observations that substantiate these effects, although no definitive quantitative assessment may be done at present. In the case of the Asian transport-impacted sample TH 1, the constant

$\Delta^{17}O$ with nitrate particle size is consistent with the relative isolation of the air mass during transport, where the nitrate formed under specific conditions that allowed precursors to homogenize, and permitted the uniform distribution of the nitrate end product over a large size range, similarly to the observations we made earlier on the sulfate.

[57] The qualitative conclusions drawn here on the aerosol formation processes are based on various assumptions and simplifications. Greater resolution in quantifying the formation budgets will be obtained when the complexity of the processes is fully taken into account. Isotope observations should be incorporated into coupled models describing the chemistry, physicochemistry and transport, and based on the gas phase and aerosol phase observations from the ITCT-2k2 campaign. In particular, the description of the aerosol burden, OH chemistry, meteorological conditions along the air mass trajectories, and observed concentrations of key species such as DMS, SO_2, H_2O_2, O_3, NO_x, VOCs, will be critical for resolving the complex aerosol formation and transformation processes. The isotopes of sulfate and nitrate, especially the $\Delta^{17}O$ anomaly in these species, will in turn introduce new dimensions to describe the aerosol formation and aging phenomena in other models.

4. Conclusions

[58] A full set of size-segregated samples collected in May 2002 alongside the ITCT-2k2 campaign at Trinidad Head (a coastal site in northern California), has been analyzed for sulfate and nitrate oxygen isotopes. The sampling was designed to study episodes of trans-Pacific transport in conjunction with other measurements deployed for the campaign. Although these measurements do not include most of the early dust events that were observed at the onset of the campaign, the data provide a number of significant new observations on background conditions at this site with respect to atmospheric chemistry and transport.

[59] The SO_4 concentration was bimodal as expected, with a fine and a coarse particle mode. The stage-averaged $\delta^{18}O$ values on the entire data set are constrained in the +7.5 to +8.9‰ range (n = 52). Individual $\delta^{18}O$ values do not exhibit systematic variability with collection date or particle size. Alternatively, the $\Delta^{17}O$ values of sulfate point to a number of original observations: (1) sulfate, which follows a bimodal distribution, contains a nonzero positive anomaly $\Delta^{17}O$ in all size fractions, consistently greater as the particle size decreases; (2) in all samples the coarse fraction sulfate exhibits a small but significant $\Delta^{17}O$ indicating a measurable uptake or in situ formation of secondary sulfate on the sea salt; (3) the formation of the non-sea-salt sulfate in the coarse fraction is consistent with two scenarios, which can be observed in the $\Delta^{17}O$ measurement: either non-sea-salt sulfate in the coarse aerosol results primarily from coagulation of finer secondary sulfate particles, when the anomaly in non-sea-salt sulfate is low and comparable in all size fractions, or it results from ozone-driven oxidation of SO_2 within the sea spray, as observed in the higher anomaly in the supermicron particles compared to the fine mode; and (4) the sample impacted by long-range transported Asian influence evidenced the importance of the coagulation process in the production of nss-SO_4 in the coarse mode in the aged air mass.

[60] In comparison to the oxygen isotopes, the sulfur isotopes of sulfate possess zero isotopic anomaly in the fine fraction, unlike what had been observed in samples from La Jolla, coastal California [*Romero and Thiemens*, 2003]. The single isotope ratio $\delta^{34}S$ confirmed the unambiguous continental origin of the fine particle sulfur observed in the Asian-impacted sample, contrary to the remainder of the samples which showed mixed anthropogenic and possibly marine biogenic origins of the non-sea-salt sulfate.

[61] The isotopic anomaly $\Delta^{17}O$ measured in size-resolved nitrate revealed for the first time differences in the budget of NO_3 formation pathways in a given air mass, as a function of particle size. The coarse nitrate consistently possessed a higher $\Delta^{17}O$ nitrate anomaly, suggesting a higher N_2O_5 hydrolysis contribution to nitrate formation budget, compared to the fine particles where homogeneous nitrate formation is proportionally more important. These new measurements are capable of providing important observations to describe finely the interactions between aerosol, cloud microphysics and the NO_y chemistry.

[62] It is noted that the lack of knowledge on the isotopic characteristics of the halogen chemistry in sulfate and nitrate formation prevents the inclusion of these potentially significant pathways in our formation budget assessment at the moment. This may be a key research area to accurately resolve the overall formation budgets of both species.

[63] The multiratio oxygen isotope measurements of sulfate and nitrate in the present study have thus far been the most comprehensive in terms of demonstrating the capability of the mass-independent signatures to elucidate aerosol formation mechanisms. Isotopic measurements of atmospheric aerosol, when viewed in conjunction with other observations such as elemental analysis, provide an essential component for determining the mode and mechanism of aerosol production, transformation, and transport. The complete multiratio isotope analysis should be a basis for future modeling of the formation and transformation processes of the soluble aerosol, based on direct observation of the mechanisms.

Appendix A: Potential Implications of Halogen Chemistry on the Isotope Tracing of Sulfate and Nitrate Formation

[64] Halogen oxide chemistry may be a major player in sulfate and nitrate formation in the troposphere, especially in the marine atmosphere where halogen compounds are readily available by activation of chlorine and bromine in sea spray or by photo-oxidation of biogenic halogen compounds [*Vogt et al.*, 1996; *Sander et al.*, 1999; *Herrmann et al.*, 2003; *Quack and Wallace*, 2003]. However, large uncertainties remain as to the relative importance of halogen chemistry in aerosol formation, due to the lack of observational evidence. In particular no direct measurement or modeling of halogen species was performed to our knowledge during ITCT-2k2. In our isotope scheme, halogen chemistry cannot be included at the moment because of the lack of knowledge from observation of the relevant isotopic mechanisms implied. We can only propose a preliminary assessment on the work to be conducted in the future to take this chemistry into account.

[65] ClO and BrO may be important gas phase oxidants of NO_2 leading to the heterogeneous production of nitrate [*Sander et al.*, 1999; *von Glasow et al.*, 2004]:

(RA1a) $$NO_2 + XO \leftrightarrow XNO_3$$

(RA1b) $$XNO_3 + H_2O(liq) \rightarrow HNO_3(aq) + HOX$$

(with X = Cl or Br). The short lifetime of $ClNO_3$ due to fast thermal decomposition does not favor the heterogeneous nitrate production from $ClNO_3$ hydrolysis [*Sander et al.*, 1999]. $BrNO_3$ on the other hand may play a nonnegligible role in heterogeneous nitrate formation. We can propose that $BrNO_3$ probably holds an isotopic anomaly retained from the precursors BrO and NO_2 if equilibrium (RA1a) is attained (the forward reaction being a termolecular reaction, and the reverse reaction caused by photodissociation), i.e., an anomaly similar to that of the ozone/NO_2 pool. It is not known at present whether the forward reaction in (RA1a) can yield an extra MIF in the halogen nitrate species produced. The subsequent hydrolysis of $BrNO_3$ may introduce one or more O atoms from the water into the final nitrate ion or nitric acid molecule. Only specific laboratory studies will be able to assess the isotopic signature to be expected from this formation pathway. This signature could then be used in models describing the full chemistry.

[66] BrO is also thought to control the DMS oxidation scheme under favorable conditions [*Toumi*, 1994; *von Glasow and Crutzen*, 2004]. The involvement of BrO in DMS oxidation does not directly interfere with our study of sulfate production as our oxygen isotope tracers are used to trace the SO_2 oxidation pathways, but brings no information from the SO_2 precursors. On the other hand, chlorine and bromine hydroxides HOX (X = Cl or Br) may be important aqueous phase oxidants of SO_2 (aq) in reaction (R2) [*Vogt et al.*, 1996; *von Glasow et al.*, 2002]. The primary production reactions of the HOX species are (RA1b) in aqueous phase, or (RA2) in the gas phase:

(RA2) $$HO_2 + XO \rightarrow HOX + O_2.$$

[67] The oxidation of SO_2(aq) with HOX was overlooked in previous studies of sulfate aerosol formation [*Savarino et al.*, 2000; *Lee and Thiemens*, 2001]. At the moment, one can only speculate on the isotope implications of this pathway, because of the lack of experimental data as to the O atom isotopic composition of HOX, and its possible isotopic exchange rate in the aqueous phase. If one considers (RA1b) to be the main production mechanism of aqueous phase HOX, the anomaly in HOX can either be very close to that of ozone (since XNO_3 can reach equilibrium with NO_2 and XO in the gas phase), or zero if the oxygen in HOX comes from water in (RA1b) or exchanges rapidly with water. An ab initio molecular dynamics study of the $ClNO_3$ hydrolysis (more precisely the reaction with the hydronium ion [*Ishikawa and Binning*, 2002]) shows that the HOCl formed may retain one O atom from the $ClNO_3$ molecule, therefore statistically bearing the same isotopic anomaly (provided the reaction does not add another anomalous effect, which is very unlikely in the aqueous phase). Another formation pathway for HOX formation is the gas phase reaction $XO + HO_2 \rightarrow XOH + O_2$ [*von Glasow et al.*, 2004]. This reaction may leave the same anomaly as that of the precursor XO in the XOH molecule, or none, depending on the mechanistic properties. We can only propose at present that if any ^{17}O anomaly exists in the dissolved HOX, one quarter of this anomaly would be transferred, similarly to the ozone mechanism, to the product sulfate following the reaction (R2): $SO_3^{2-} + HOX \rightarrow SO_4^{2-} + HX$.

[68] As a consequence of all the uncertainties described, the participation of HOBr and HOCl in sulfate formation, and of $BrNO_3$ in nitrate formation, will only be assessed in further studies, as viewed through relevant experimental observations. These oxidation pathways will then be associated either with the processes yielding a high anomaly in the end product in the formation budgets presented above (ozone oxidation for SO_4, or (R4) pathway for nitrate), or as a low anomaly one in aqueous phase formation, depending on the characteristic isotopic signatures of each pathway. Either way, the formation budgets proposed here will need to be revised accordingly.

[69] **Acknowledgments.** The authors gratefully acknowledge Jose Montoya for sample collection at Trinidad Head and NOAA staff for site setup and support. The authors acknowledge the NSF for partial support of this work. S.S.C. acknowledges funding from the NOAA Climate Program Office under grant NA16GP2360.

References

Alexander, B., R. J. Park, D. J. Jacob, Q. B. Li, R. M. Yantosca, J. Savarino, C. C. W. Lee, and M. H. Thiemens (2005), Sulfate formation in sea-salt aerosols: Constraints from oxygen isotopes, *J. Geophys. Res.*, *110*, D10307, doi:10.1029/2004JD005659.

Allan, J. D., et al. (2004), Submicron aerosol composition at Trinidad Head, California, during ITCT 2K2: Its relationship with gas phase volatile organic carbon and assessment of instrument performance, *J. Geophys. Res.*, *109*, D23S24, doi:10.1029/2003JD004208.

Anttila, T., A. Kiendler-Scharr, R. Tillmann, and T. F. Mentel (2006), On the reactive uptake of gaseous compounds by organic-coated aqueous aerosols: Theoretical analysis and application to the heterogeneous hydrolysis of N_2O_5, *J. Phys. Chem. A*, *110*, 10,435–10,443.

Bao, H., and M. C. Reheis (2003), Multiple oxygen and sulfur isotopic analyses on water-soluble sulfate in bulk atmospheric deposition from the southwestern United States, *J. Geophys. Res.*, *108*(D14), 4430, doi:10.1029/2002JD003022.

Bao, H., and M. H. Thiemens (2000), Generation of O_2 from $BaSO_4$ using a CO_2-laser fluorination system for simultaneous $\delta^{18}O$ and $\delta^{17}O$ analysis, *Anal. Chem.*, *72*(17), 4029–4032.

Baroni, M., M. H. Thiemens, R. J. Delmas, and J. Savarino (2007), Mass-independent sulfur isotopic compositions in stratospheric volcanic eruptions, *Science*, *315*, 84–87.

Boucher, O., and M. Pham (2002), History of sulfate aerosol radiative forcings, *Geophys. Res. Lett.*, *29*(9), 1308, doi:10.1029/2001GL014048.

Brenninkmeijer, C. A. M., C. Janssen, J. Kaiser, T. Röckmann, T. S. Rhee, and S. S. Assonov (2003), Isotope effects in the chemistry of atmospheric trace compounds, *Chem. Rev.*, *103*, 5125–5161.

Charlson, R. J., J. E. Lovelock, M. O. Andreae, and S. G. Warren (1987), Oceanic phytoplankton, atmospheric sulphur, cloud albedo and climate, *Nature*, *326*, 655–661.

Chuck, A. L., S. M. Turner, and P. S. Liss (2002), Direct evidence for a marine source of C_1 and C_2 alkyl nitrates, *Science*, *297*, 1151–1154.

DeBell, L. J., M. Vozzella, R. W. Talbot, and J. E. Dibb (2004), Asian dust storm events of spring 2001 and associated pollutants observed in New England by the Atmospheric Investigation, Regional Modeling, Analysis and Prediction (AIRMAP) monitoring network, *J. Geophys. Res.*, *109*, D01304, doi:10.1029/2003JD003733.

Farquhar, J., H. Bao, and M. H. Thiemens (2000a), Atmospheric influence of earth's earliest sulfur cycle, *Science*, *289*, 756–758.

Farquhar, J., T. L. Jackson, and M. H. Thiemens (2000b), A ^{33}S enrichment in ureilite meteorites: Evidence for a nebular sulfur component, *Geochim. Cosmochim. Acta*, *64*(10), 1819–1825.

Fehsenfeld, F. C., et al. (2006), International Consortium for Atmospheric Research on Transport and Transformation (ICARTT): North America to Europe–Overview of the 2004 summer field study, *J. Geophys. Res.*, *111*, D23S01, doi:10.1029/2006JD007829.

Gao, Y. Q., and R. A. Marcus (2001), Strange and unconventional isotope effects in ozone formation, *Science*, *293*, 259–263.

Goldstein, A. H., D. B. Millet, M. McKay, L. Jaeglé, L. Horowitz, O. Cooper, R. Hudman, D. J. Jacob, S. Oltmans, and A. Clarke (2004), Impact of Asian emissions on observations at Trinidad Head, California, during ITCT 2K2, *J. Geophys. Res.*, *109*, D23S17, doi:10.1029/2003JD004406.

Gong, S. L., and L. A. Barrie (2003), Simulating the impact of sea salt on global nss sulphate aerosols, *J. Geophys. Res.*, *108*(D16), 4516, doi:10.1029/2002JD003181.

Gurciullo, C., B. Lerner, H. Sievering, and S. N. Pandis (1999), Heterogeneous sulfate production in the remote marine environment: Cloud processing and sea-salt particle contributions, *J. Geophys. Res.*, *104*(D17), 21,719–21,731.

Herrmann, H., Z. Majdik, B. Ervens, and D. Weise (2003), Halogen production from aqueous tropospheric particles, *Chemosphere*, *52*, 485–502.

Holt, B. D., R. Kumar, and P. T. Cunningham (1981), Oxygen-18 study of the aqueous-phase oxidation of sulfur dioxide, *Atmos. Environ.*, *15*(4), 557–566.

Huebert, B. J., T. Bates, P. B. Russell, G. Shi, Y. J. Kim, K. Kawamura, G. Carmichael, and T. Nakajima (2003), An overview of ACE-Asia: Strategies for quantifying the relationships between Asian aerosols and their climatic impacts, *J. Geophys. Res.*, *108*(D23), 8633, doi:10.1029/2003JD003550.

Husar, R. B., et al. (2001), Asian dust events of April 1998, *J. Geophys. Res.*, *106*(D16), 18,317–18,330.

Hwang, H. J., and C. U. Ro (2006), Direct observation of nitrate and sulfate formations from mineral dust and sea-salts using low-Z particle electron probe X-ray microanalysis, *Atmos. Environ.*, *40*, 3869–3880.

Ishikawa, Y., and R. C. Binning Jr. (2002), Ab initio direct molecular dynamics study of $ClONO_2 + H_3O^+$, *Chem. Phys. Lett.*, *358*, 509–515.

Johnson, M. S., K. L. Feilberg, P. von Hessberg, and O. J. Nielsen (2002), Isotopic processes in atmospheric chemistry, *Chem. Soc. Rev.*, *31*, 313–323.

Johnston, J. C., and M. H. Thiemens (1997), The isotopic composition of tropospheric ozone in three environments, *J. Geophys. Res.*, *102*(D21), 25,395–25,404.

Kaiser, J., T. Röckmann, and C. A. M. Brenninkmeijer (2004), Contribution of mass-dependent fractionation to the oxygen isotope anomaly of atmospheric nitrous oxide, *J. Geophys. Res.*, *109*, D03305, doi:10.1029/2003JD004088.

Karagulian, F., C. Santschi, and M. J. Rossi (2006), The heterogeneous chemical kinetics of N_2O_5 on $CaCO_3$ and other atmospheric mineral dust surrogates, *Atmos. Chem. Phys.*, *6*, 1373–1388.

Krankowsky, D., F. Bartecki, G. G. Klees, K. Mauersberger, K. Schellenbach, and J. Stehr (1995), Measurement of heavy isotope enrichment in tropospheric ozone, *Geophys. Res. Lett.*, *22*(13), 1713–1716.

Krankowsky, D., P. Lämmerzahl, K. Mauersberger, C. Janssen, B. Tuzson, and T. Röckmann (2007), Stratospheric ozone isotope fractionations derived from collected samples, *J. Geophys. Res.*, *112*, D08301, doi:10.1029/2006JD007855.

Kreutz, K. J., and E. R. Sholkovitz (2000), Major element, rare earth element, and sulfur isotopic composition of a high-elevation firn core: Sources and transport of mineral dust in central Asia, *Geochem. Geophys. Geosyst.*, *1*(11), doi:10.1029/2000GC000082.

Lämmerzahl, P., T. Röckmann, C. A. M. Brenninkmeijer, D. Krankowsky, and K. Mauersberger (2002), Oxygen isotope composition of stratospheric carbon dioxide, *Geophys. Res. Lett.*, *29*(12), 1582, doi:10.1029/2001GL014343.

Laskin, A., D. J. Gaspar, W. Wang, S. W. Hunt, J. P. Cowin, S. D. Colson, and B. J. Finlayson-Pitts (2003), Reactions at interfaces as a source of sulfate formation in sea-salt particles, *Science*, *301*, 340–344.

Lee, C. C. W., and M. H. Thiemens (2001), The $\delta^{17}O$ and $\delta^{18}O$ measurements of atmospheric sulfate from a coastal and high alpine region: A mass-independent isotopic anomaly, *J. Geophys. Res.*, *106*(D15), 17,359–17,373.

Longinelli, A., and H. Craig (1967), Oxygen-18 variations in sulfate ions in sea water and saline lakes, *Science*, *156*, 56–59.

Luz, B., and E. Barkan (2005), The isotopic ratios $^{17}O/^{16}O$ and $^{18}O/^{16}O$ in molecular oxygen and their significance in biogeochemistry, *Geochim. Cosmochim. Acta*, *69*(5), 1099–1110, doi:10.1016/j.gca.2004.09.001.

Lyons, R. L. (2001), Transfer of mass-independent fractionation in ozone to other oxygen-containing radicals in the atmosphere, *Geophys. Res. Lett.*, *28*(17), 3231–3234.

Malm, W. C., J. F. Sisler, D. Huffman, R. A. Eldred, and T. A. Cahill (1994), Spatial and seasonal trends in particle concentration and optical extinction in the United States, *J. Geophys. Res.*, *99*(D1), 1347–1370.

Malm, W. C., B. A. Schichtel, M. L. Pitchford, L. L. Ashbaugh, and R. A. Eldred (2004), Spatial and monthly trends in speciated fine particle concentration in the United States, *J. Geophys. Res.*, *109*, D03306, doi:10.1029/2003JD003739.

Mentel, T. F., M. Sohn, and A. Wahner (1999), Nitrate effect in the heterogeneous hydrolysis of dinitrogen pentoxide on aqueous aerosols, *Phys. Chem. Chem. Phys.*, *1*(24), 5451–5457.

Michalski, G., J. Savarino, J. K. Böhlke, and M. H. Thiemens (2002), Determination of the total oxygen isotopic composition of nitrate and the calibration of a $\Delta^{17}O$ nitrate reference material, *Anal. Chem.*, *74*, 4989–4993.

Michalski, G., Z. Scott, M. Kabiling, and M. H. Thiemens (2003), First measurements and modeling of $\Delta^{17}O$ in atmospheric nitrate, *Geophys. Res. Lett.*, *30*(16), 1870, doi:10.1029/2003GL017015.

Miller, M. F. (2002), Isotopic fractionation and the quantification of ^{17}O anomalies in the oxygen three-isotope system: An appraisal and geochemical significance, *Geochim. Cosmochim. Acta*, *66*(11), 1881–1889.

Millet, D. B., et al. (2004), Volatile organic compound measurements at Trinidad Head, California, during ITCT 2K2: Analysis of sources, atmospheric composition, and aerosol residence times, *J. Geophys. Res.*, *109*, D23S16, doi:10.1029/2003JD004026.

Norman, A. L., L. A. Barrie, D. Toom-Sauntry, A. Sirois, H. R. Krouse, S. M. Li, and S. Sharma (1999), Sources of aerosol sulphate at Alert: Apportionment using stable isotopes, *J. Geophys. Res.*, *104*(D9), 11,619–11,631.

Norman, A. L., W. Belzer, and L. A. Barrie (2004), Insights into the biogenic contribution to total sulphate in aerosol and precipitation in the Fraser Valley afforded by isotopes of sulphur and oxygen, *J. Geophys. Res.*, *109*, D05311, doi:10.1029/2002JD003072.

Parrish, D. D., Y. Kondo, O. R. Cooper, C. A. Brock, D. A. Jaffe, M. Trainer, T. Ogawa, G. Hübler, and F. C. Fehsenfeld (2004), Intercontinental Transport and Chemical Transformation 2002 (ITCT2K2) and Pacific Exploration of Asian Continental Emission (PEACE) experiments: An overview of the 2002 winter and spring intensives, *J. Geophys. Res.*, *109*, D23S01, doi:10.1029/2004JD004980.

Patris, N., N. Mihalopoulos, E. D. Baboukas, and J. Jouzel (2000), Isotopic composition of sulfur in size-resolved marine aerosols above the Atlantic Ocean, *J. Geophys. Res.*, *105*(D11), 14,449–14,457.

Patris, N., R. Delmas, M. Legrand, M. De Angelis, F. A. Ferron, M. Stiévenard, and J. Jouzel (2002), First sulfur isotope measurements in central Greenland ice cores along the preindustrial and industrial periods, *J. Geophys. Res.*, *107*(D11), 4115, doi:10.1029/2001JD000672.

Perry, K. D., S. S. Cliff, and M. P. Jimenez-Cruz (2004), Evidence for hygroscopic mineral dust particles from the Intercontinental Transport and Chemical Transformation experiment, *J. Geophys. Res.*, *109*, D23S28, doi:10.1029/2004JD004979.

Pham, M., O. Boucher, and D. Hauglustaine (2005), Changes in atmospheric sulfur burdens and concentrations and resulting radiative forcings under IPCC SRES emission scenarios for 1990–2100, *J. Geophys. Res.*, *110*, D06112, doi:10.1029/2004JD005125.

Pruett, L. E., K. J. Kreutz, M. Wadleigh, and V. Aizen (2004), Assessment of sulfate sources in high-elevation Asian precipitation using stable sulfur isotopes, *Environ. Sci. Technol.*, *38*, 4728–4733.

Quack, B., and D. W. R. Wallace (2003), Air-sea flux of bromoform: Controls, rates, and implications, *Global Biogeochem. Cycles*, *17*(1), 1023, doi:10.1029/2002GB001890.

Raes, F., R. Van Dingenen, E. Vignati, J. Wilson, J. P. Putaud, J. H. Seinfeld, and P. Adams (2000), Formation and cycling of aerosols in the global troposphere, *Atmos. Environ.*, *34*, 4215–4240.

Ramanathan, V., et al. (2001), Indian Ocean Experiment: An integrated analysis of the climate forcing and effects of the great Indo-Asian haze, *J. Geophys. Res.*, *106*(D22), 28,371–28,398.

Romero, A. B., and M. H. Thiemens (2003), Mass-independent sulfur isotopic compositions in present-day sulfate aerosols, *J. Geophys. Res.*, *108*(D16), 4524, doi:10.1029/2003JD003660.

Sander, R., Y. Rudich, R. von Glasow, and P. J. Crutzen (1999), The role of $BrNO_3$ in marine tropospheric chemistry: A model study, *Geophys. Res. Lett.*, *26*(18), 2857–2860.

Santschi, C., and M. J. Rossi (2006), Uptake of CO_2, SO_2, HNO_3 and HCl on calcite ($CaCO_3$) at 300 K: Mechanism and the role of adsorbed water, *J. Phys. Chem. A*, *110*(21), 6789–6802.

Saul, T. D., M. P. Tolocka, and M. V. Johnston (2006), Reactive uptake of nitric acid onto sodium chloride aerosols across a wide range of relative humidities, *J. Phys. Chem. A*, *110*(24), 7614–7620.

Savarino, J., and M. H. Thiemens (1999), Analytical procedure to determine both $\delta^{18}O$ and $\delta^{17}O$ of H_2O_2 in natural water and first measurements, *Atmos. Environ.*, *33*, 3683–3690.

Savarino, J., C. C. W. Lee, and M. H. Thiemens (2000), Laboratory oxygen isotopic study of sulfur (IV) oxidation: Origin of the mass-independent oxygen isotopic anomaly in sulfates and sulfate mineral deposits on Earth, *J. Geophys. Res.*, *105*(D23), 29,079–29,088.

Savarino, J., B. Alexander, V. Darmohusodo, and M. H. Thiemens (2001), Sulfur and oxygen isotope analysis of sulfate at micromole levels using a pyrolysis technique in a continuous flow system, *Anal. Chem.*, *73*, 4457–4462.

Savoie, D. L., R. Arimoto, W. C. Keene, J. M. Prospero, R. A. Duce, and J. N. Galloway (2002), Marine biogenic and anthropogenic contributions to non-sea-salt sulfate in the marine boundary layer over the North Atlantic Ocean, *J. Geophys. Res.*, *107*(D18), 4356, doi:10.1029/2001JD000970.

Schueler, B., J. Morton, and K. Mauersberger (1990), Measurement of isotopic abundances in collected stratospheric ozone samples, *Geophys. Res. Lett.*, *17*(9), 1295–1298.

Sievering, H., B. Lerner, J. Slavich, J. Anderson, M. Posfai, and J. Cainey (1999), O_3 oxidation of SO_2 in sea-salt aerosol water: Size distribution of non-sea-salt sulfate during the First Aerosol Characterization Experiment (ACE 1), *J. Geophys. Res.*, *104*(D17), 21,707–21,717.

Sievering, H., J. Cainey, M. Harvey, J. McGregor, S. Nichol, and P. Quinn (2004), Aerosol non-sea-salt sulfate in the remote marine boundary layer under clear-sky and normal cloudiness conditions: Ocean-derived biogenic alkalinity enhances sea-salt sulfate production by ozone oxidation, *J. Geophys. Res.*, *109*, D19317, doi:10.1029/2003JD004315.

Tang, Y., et al. (2004), Multiscale simulations of tropospheric chemistry in the eastern Pacific and on the U. S. West Coast during spring 2002, *J. Geophys. Res.*, *109*, D23S11, doi:10.1029/2004JD004513.

Thiemens, M. H. (1999), Mass-independent isotope effects in planetary atmospheres and the solar system, *Science*, *283*, 341–345.

Thiemens, M. H. (2002), Mass-independent isotope effects and their use in understanding natural processes, *Isr. J. Chem.*, *42*, 43–54.

Thiemens, M. H., T. L. Jackson, and C. A. M. Brenninkmeijer (1995), Observation of a mass independent oxygen isotopic composition in terrestrial stratospheric CO_2, the link to ozone chemistry, and the possible occurrence in the Martian atmosphere, *Geophys. Res. Lett.*, *22*(3), 255–258.

Thiemens, M. H., J. Savarino, J. Farquhar, and H. Bao (2001), Mass-independent isotopic compositions in terrestrial and extraterrestrial solids and their applications, *Account. Chem. Res.*, *34*(8), 645–652.

Tie, X., et al. (2003), Effect of sulfate aerosol on tropospheric NO_x and ozone budgets: Model simulations and TOPSE evidence, *J. Geophys. Res.*, *108*(D4), 8364, doi:10.1029/2001JD001508.

Toumi, R. (1994), BrO as a sink for dimethylsulfide in the marine atmosphere, *Geophys. Res. Lett.*, *21*(2), 117–120.

van den Berg, A., F. Dentener, and J. Lelieveld (2000), Modeling the chemistry of the marine boundary layer: Sulphate formation and the role of sea-salt aerosol particles, *J. Geophys. Res.*, *105*(D9), 11,671–11,698.

VanCuren, R. A. (2003), Asian aerosols in North America: Extracting the chemical composition and mass concentration of the Asian continental aerosol plume from long-term aerosol records in the western United States, *J. Geophys. Res.*, *108*(D20), 4623, doi:10.1029/2003JD003459.

VanCuren, R., and T. Cahill (2002), Asian aerosols in North America: Frequency and concentration of fine dust, *J. Geophys. Res.*, *107*(D24), 4804, doi:10.1029/2002JD002204.

VanCuren, R. A., S. S. Cliff, K. D. Perry, and M. Jimenez-Cruz (2005), Asian continental aerosol persistence above the marine boundary layer over the eastern North Pacific: Continuous aerosol measurements from Intercontinental Transport and Chemical Transformation 2002 (ITCT 2K2), *J. Geophys. Res.*, *110*(D9), D09S90, doi:10.1029/2004JD004973.

Vlasenko, A., S. Sjogren, E. Weingartner, K. Stemmler, H. W. Gaggeler, and M. Ammann (2006), Effect of humidity on nitric acid uptake to mineral dust aerosol particles, *Atmos. Chem. Phys.*, *6*, 2147–2160.

Vogt, R., P. J. Crutzen, and R. Sander (1996), A mechanism for halogen release from sea-salt aerosol in the remote marine boundary layer, *Nature*, *383*, 327–330.

von Glasow, R., and P. J. Crutzen (2004), Model study of multiphase DMS oxidation with a focus on halogens, *Atmos. Chem. Phys.*, *4*, 589–608.

von Glasow, R., R. Sander, A. Bott, and P. J. Crutzen (2002), Modeling halogen chemistry in the marine boundary layer: 2. Interactions with sulfur and the cloud-covered MBL, *J. Geophys. Res.*, *107*(D17), 4323, doi:10.1029/2001JD000943.

von Glasow, R., R. von Kuhlmann, M. G. Lawrence, U. Platt, and P. J. Crutzen (2004), Impact of reactive bromine chemistry in the troposphere, *Atmos. Chem. Phys.*, *4*, 2481–2497.

Young, E. D., A. Galy, and H. Nagahara (2002), Kinetic and equilibrium mass-dependent isotope fractionation laws in nature and their geochemical and cosmochemical significance, *Geochim. Cosmochim. Acta*, *66*(6), 1095–1104.

Yu, J. Y., and Y. Park (2004), Sulphur isotopic and chemical compositions of the natural waters in the Chuncheon area, Korea, *Appl. Geochem.*, *19*(6), 843–853.

S. S. Cliff, Department of Applied Sciences, University of California, Davis, CA 95616, USA.

M. Kasem and M. H. Thiemens, Department of Chemistry and Biochemistry, University of California, San Diego, 9500 Gilman Drive, La Jolla, CA 92093-0356, USA.

N. Patris, Institut de Recherche pour le Développement, UR032 Great Ice, MSE, Université Montpellier 2, CC 57, F-34095 Montpellier, France. (npatris@msem.univ-montp2.fr)

P. K. Quinn, Pacific Marine Environmental Laboratory, NOAA, Seattle, WA 98115, USA.